Hybrid event bed character and distribution in the context of ancient deep-lacustrine fan models

THOMAS J. H. DODD*,† iD, DAVE J. MCCARTHY* iD, LAWRENCE AMY‡ iD,
GAYLE E. PLENDERLEITH* iD and STUART M. CLARKE†*
*British Geological Survey, the Lyell Centre, Research Avenue South, Edinburgh, EH144AP, UK
(E-mail: tdodd@bgs.ac.uk)
†Basin Dynamics Research Group, School of Geography, Geology and Environment, Keele University,
Keele, Staffordshire, ST55BG, UK
‡School of Earth Sciences, University College Dublin, Belfield, Dublin 4, Ireland

ABSTRACT

Hybrid event beds are texturally and compositionally-diverse deposits preserved within deepwater settings. They are deposited by flows exhibiting 'mixed behaviour', forming complex successions of sandstone and mudstone, which are often challenging to predict. Hybrid event beds are documented in deep-marine settings, where they have been thoroughly characterized, and are well-known as effective fluid transmissibility barriers and baffles in reservoirs. By comparison, there are far-fewer studies of hybrid event beds from deep-lacustrine settings, where their character and distribution remains relatively under-explored. In order to provide insights into these deposits, this study presents the detailed analysis of three-dimensional seismic data, wireline logs and core from a series of ancient deep-lacustrine fan systems in the North Falkland Basin. Results confirm that deep-lacustrine hybrid event beds comprise the same idealized sequence of the 'H1–H5' divisions. However, in this study H3 'debrite' units can be subdivided into 'H3a–H3c', based on: sharp or erosional intra-H3 contacts, bulk lithology, mud-content and discrete sedimentary textures. This study interprets the H3a–H3c sub-units as the products of multiple flow components formed through significant rearward longitudinal flow transformation processes, during the emplacement of a single hybrid event bed. Hybrid event beds are observed within lobe fringes, where flow types, energies and transport mechanisms diversify as a result of flow transformation. The temporal context of hybrid event bed occurrences is considered in relation to stages of fan evolution, including: the Initiation; Growth (I); Growth (II); By-pass; Abandonment; and Termination phases. Hybrid event beds are mainly found in either the initiation phase where flow interaction and erosion of initial substrates promoted mixed flow behaviour, or in the abandonment phase as facies belts retreated landward. The results of this study have important implications in terms of flow processes of hybrid event bed emplacement, in particular sub-division of the H3 unit, as well as the prediction of hybrid event bed occurrence and character within ancient deep-lacustrine fan settings, in general.

Keywords Deep-lacustrine, fan models, hybrid event beds, mixed flow behaviour, North Falkland Basin, turbidites.

INTRODUCTION

A variety of subaqueous sediment gravity-driven flow types are recognized in deepwater environments, including: cohesive flows; non-cohesive flows such as hyper-concentrated, hyper-concentrated-grain-flows and concentrated-sediment-gravity-flows/density-flows (*sensu* Lowe, 1982; Pierson & Costa, 1987; Mulder & Alexander, 2001); flows with some component of fluid turbulence, which can be sub-divided into high-density turbidity currents and low-density turbidity currents (Lowe, 1982); and flows that show mixed behaviour (*sensu* Haughton *et al.*, 2009), or transitional flows (*sensu* Kane & Pontén, 2012; Kane *et al.*, 2017). This broad range of flow types were defined using examples from deep-marine settings, and they also occur within deep-lacustrine environments (Baganz *et al.*, 2012; Dodd *et al.*, 2019; Yang *et al.*, 2019). Subaqueous sediment gravity flows in deep-lacustrine basins can deposit clean, well-sorted sandstones with excellent reservoir potential (Horton & Schmitt, 1996; Baganz *et al.*, 2012; Dodd *et al.*, 2019; Zhang *et al.*, 2019; Pan *et al.*, 2020).

In particular, hybrid event beds (HEBs) represent widely-recognized deposits, formed by, or under, flows that exhibited 'mixed', 'transitional', or what is also referred to as 'hybrid' flow behaviour (*sensu* Haughton *et al.*, 2003, 2009; Kane & Pontén, 2012). They form texturally and compositionally-diverse deposits preserved within deepwater settings (Porten *et al.*, 2016; Southern *et al.*, 2017), which are often mud-rich, and can act as significant fluid barriers or baffles (Haughton *et al.*, 2003; Amy & Talling, 2006; Amy *et al.*, 2009; Davis *et al.*, 2009; Kane & Pontén, 2012; Fonnesu *et al.*, 2015). Hybrid flow deposits have a wide-range of terminology applied, including: slurry flows/beds (Ricci Lucchi & Valmori, 1980; Lowe & Guy, 2000; Tinterri & Piazza, 2019); transitional flow deposits (Kane & Pontén, 2012); hybrid beds (Kane *et al.*, 2017; Bell *et al.*, 2018; Hansen *et al.*, 2019); matrix-rich beds (Terlaky & Arnott, 2014); clay-rich flows (Barker *et al.*, 2008); linked-debrites; and HEBs (Haughton *et al.*, 2003, 2009; Amy & Talling, 2006; Hodgson, 2009; Sumner *et al.*, 2009; Patacci *et al.*, 2014, 2020; Fonnesu *et al.*, 2015, 2016, 2018; Southern *et al.*, 2015, 2017; Porten *et al.*, 2016; Pierce *et al.*, 2018; Baker & Baas, 2020; Hussain *et al.*, 2020). These flow types have been modelled experimentally (Baas *et al.*, 2009, 2011; Sumner *et al.*, 2009, 2012). Despite being well-documented in marine environments (Haughton *et al.*, 2009; Pierce *et al.*, 2018), and HEB distribution and character widely explored (Hodgson *et al.*, 2006; Davis *et al.*, 2009; Kane *et al.*, 2017; Spychala *et al.*, 2017a,b; Bell *et al.*, 2018; Pierce *et al.*, 2018; Baas *et al.*, 2021), their occurrence and variability in deep-lacustrine fan settings is less understood, with there being few published examples (Hovikoski, *et al.*, 2016; Tan *et al.*, 2017; Dodd *et al.*, 2019; Yang *et al.*, 2019; Shan *et al.*, 2020; Zhang & Dong, 2020).

The HEB model (Haughton *et al.*, 2009) describes flow transformation from an initially turbulent, or at least turbulence-supressed, non-cohesive flow, into more-cohesive regimes, facilitated by flow deceleration and/or inclusion of fines through erosion, dispersal and/or fractionation of mud (already within a flow), which acts to suppress fluid-turbulence. Therefore, the generation of a HEB (through inclusion of mud) is thought to have a number of possible mechanisms, including: up-dip turbulent erosion of the substrate over which the flows are passing (Haughton *et al.*, 2003, 2009; Fonnesu *et al.*, 2018); or substrate de-lamination and erosion of mud-clasts from the basin-floor that become incorporated in the flow (*sensu* Fonnesu *et al.*, 2016).

Hybrid event beds are divided into five key, idealized internal divisions, termed H1 to H5 (Fig. 1A; Haughton *et al.*, 2009): H1 comprises clean structureless high-density turbidite sandstones; H2 is a banded sandstone formed of alternating light and dark layers through bedform development under transitional flow conditions (*sensu* Baas *et al.*, 2011; Stevenson *et al.*, 2020); H3 is typically a mud-rich debritic sandstone; H4 is a thin graded sandstone and siltstone with common parallel and ripple lamination related to low-density flows of the turbulent wake; and H5 is a mudstone cap formed by suspension fall-out (*sensu* Haughton *et al.*, 2009; Hussain *et al.*, 2020). H1 has been sub-divided into H1a and H1b (Fonnesu *et al.*, 2015; Pierce *et al.*, 2018).

In particular, the H3 unit is considered as the product of a cohesive debris flow, with upward increase in mud-matrix content associated with longitudinal heterogeneity in the passing flow (Haughton *et al.*, 2003, 2009; Hussain *et al.*, 2020; Baas *et al.*, 2021). Haughton *et al.* (2009) described H3 as "a complex mixture of sandy mudstone or muddy sandstone with or without mud-clasts, sand injections, 'sand patches',
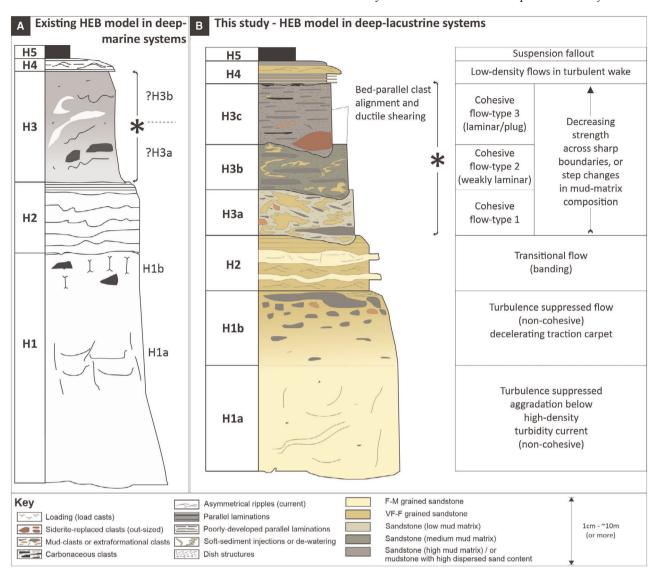
Fig. 1. Idealized sedimentary models for deep-lacustrine fan systems (A) The hybrid event bed (HEB) model redrawn after Haughton *et al.* (2009), modified after Pierce *et al.* (2018) and Hussain *et al.* (2020). It comprises five sub-divisions H1 to H5. H3, the key unit investigated in this study, is marked by an asterisk symbol. (B) The hybrid event bed model, as proposed in this study, which focusses on further sub-division of the H3 unit into 'H3a, H3b and H3c', based on sharp, erosional or loaded internal H3 contacts *(BGS © UKRI 2022)*.

outsized granules and shear fabrics, and often displays a segregation of carbonaceous fragments to the top where they are sometimes laminated". Mud-clasts are often elongate, and can either define a bedding-parallel fabric, or more chaotic arrangements. Plant fragments or carbonaceous material are common in the H3 division, especially near to the top of the H3 unit (Haughton *et al.*, 2009; Hodgson, 2009; Tan *et al.*, 2017; Yang *et al.*, 2019). A sub-division of the H3 unit was recognized in Terlaky & Arnott (2014), where matrix-rich sandstones (i.e. H3), were

divided into: structureless matrix-rich sand-stone; matrix-rich sandstone capped by matrix poor wavy or parallel laminated sandstone (the latter essentially representing H4); matrix-rich sandstone with mud-clasts; and matrix-rich sandstone with an 'abrupt increase in matrix content'. Debritic units (H3) with sub-divisions, sharp contacts and textural variability were also recognized elsewhere (Kane *et al.*, 2017; Bell *et al.*, 2018). Fonnesu *et al.* (2018) divided a succession of HEBs into six 'bed types' (HEB-1 to HEB-6), based on "differences in texture of

the muddier and chaotic division", and therefore recognized internal variability within the H3 unit. More recently, H3 has been sub-divided into two sub-units (H3a and H3b) and possible flow processes have been discussed (Hussain *et al.*, 2020; Baas *et al.*, 2021). The observed internal variation of the H3 unit, as illustrated above, suggests that an improved understanding of debrite emplacement processes during mixed flow behaviour events is still required.

In order to examine the character of deep-lacustrine HEBs, document their internal variability and likely sedimentary emplacement processes (in particular the H3 unit), and place them in the context of deep-lacustrine fan systems (both spatially and temporally), this study investigates a suite of 3D seismic, wireline data and continuous core from the North Falklands Basin (NFB), Falkland Islands (Fig. 2A). The examined systems include the early Cretaceous-aged Casper, Zebedee and Beverley fans (Fig. 3). Through examining these data, this study addressed the following key questions:

1 What is the sedimentary character of HEBs in a deep-lacustrine fan setting?
2 Can deep-lacustrine HEBs be sub-divided and what processes lead to the deposition of their constituent components?
3 What is the character and spatial context of HEBs in-relation to the coarse-grained deep-lacustrine fan model?
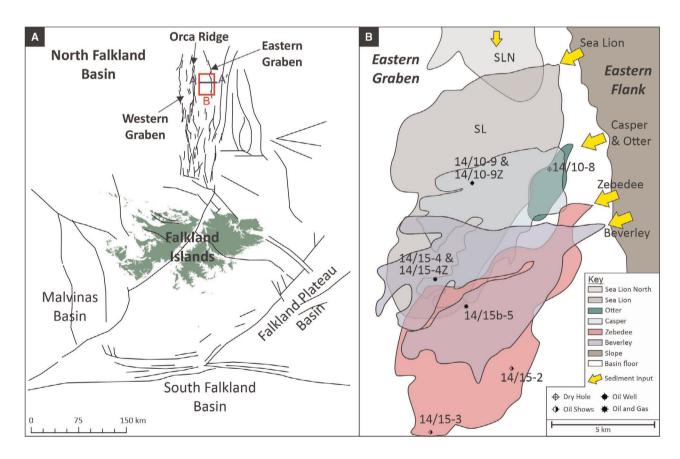**4** What is the temporal distribution of HEBs in relation to a fan evolution model?

Fig. 2. Location maps and fan outlines. (A) The Falkland Islands and four offshore sedimentary basins: Malvinas Basin, South Falkland Basin, Falkland Plateau Basin and the North Falklands Basin (NFB). The NFB comprises a number of different offset depocentres; however, this study focusses on the 'Eastern Graben'. The location of line A–A' in Fig. 3 is shown, represented by an east–west profile across the area of interest; red bock denotes position of (B). (B) Mapped polygons that outline the distribution or known extent of the Casper, Zebedee and Beverley fans of this study. For context, the position and known distributions of the Sea Lion North (SLN), Sea Lion and Otter fans have been provided. Three key sediment entry points are shown on these maps with the Sea Lion feeder representing the most northerly point, Otter and Casper sharing an input point, with Zebedee and Beverley entering the basin from the southern-most channel *(BGS © UKRI 2022)*.
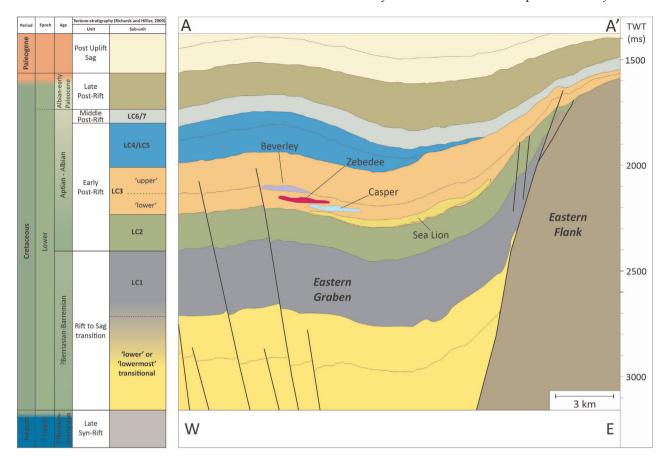
Fig. 3. Stratigraphic framework for the North Falklands Basin, and accompanying east–west oriented geoseismic line showing the overall structure of the Eastern Graben. The stratigraphic position of the fans contained within the study has been marked, all within the LC3 unit *(BGS © UKRI 2022)*.

5 What are the fundamental controls on the spatial and temporal occurrence of HEBs, and their variation in character?

Through this analysis, this study provides important insights into HEB character, likely emplacement processes, and relates their occurrence and distribution to the wider-context of depositional models for deep-lacustrine turbidite fans.

GEOLOGICAL BACKGROUND

Geological setting

The NFB, a Mesozoic-aged sedimentary basin located north of the Falkland Islands (Fig. 2A), is an intracontinental rift system, displaying two dominant structural trends: north–south oriented faulting in the basin's northern area; and north-west/south-east oriented faults in the south. The northern area has a half-graben geometry with the depocentre-controlling faults located on its eastern margin (Richards *et al.*, 1996a,b; Richards & Fannin, 1997; Richards & Hillier, 2000; Lohr & Underhill, 2015; Jones *et al.*, 2019). Rifting initiated some time in the Jurassic, associated with the break-up of Gondwana, and progressed into the early Cretaceous. In the northern area, the central rift system is divided into two depocentres termed the Western and Eastern grabens, separated by the Orca Ridge. The central rift system is approximately 125 km long, from north to south, 75 km wide from west to east, and is surrounded by a number of laterally-adjacent sub-basins (Fig. 2A; Jones *et al.*, 2019). Multiple episodes of rifting are recorded by different syn-rift packages (Richards & Hillier, 2000; Lohr & Underhill, 2015).

After the initial rifting, the basin underwent a thermal sag phase during Berriasian–Valanginian times, which formed the transitional unit (Fig. 3; Richards & Hillier, 2000). This was followed by the deposition of a >1 km thick early post-rift unit, comprising the Lower Cretaceous ('LC') LC2, LC3 and LC4 sub-units (Richards & Hillier, 2000); an interval deposited during a time when a deep-lake occupied the NFB (Richards & Hillier, 2000). The early post-rift contains many examples of margin-fed turbidite fan systems, such as the Sea Lion Fan (Williams, 2015; Dodd *et al.*, 2019). The early post-rift is overlain by middle and late post-rift units (Richards & Hillier, 2000), followed by a 'post-uplift sag' unit (Richards & Hillier, 2000).

Early post-rift deep-lacustrine fans in the North Falklands Basin

A variety of deep-lacustrine fans were deposited during different post-rift phases of the NFB, with some examples including: Liz, Beth and Rachel (Richards *et al.*, 2006), Sea Lion, Zebedee, and Casper (MacAulay, 2015); and Sea Lion North and Otter (Dodd *et al.*, 2019). The LC3 Sea Lion Fan (Bunt, 2015; Williams, 2015; Dodd *et al.*, 2019) represents the best understood system in the NFB, comprising three lobes: Sea Lion 10 (SL10); Sea Lion 15 (SL15); and Sea Lion 20 (SL20; *sensu* Dodd *et al.*, 2019). The lobes form a series of compensationally-offset stacked, tabular deposits that exhibit a complex suite of seismic amplitude 'geometries' or 'architectures' in plan-view. Internally, the lobes comprise a series of high-density turbidites, low-density turbidites and HEBs, interbedded within hemi-limnic mudstones (Dodd *et al.*, 2019).

This study focusses on the Cretaceous-aged Casper Beverley and Zebedee fans (Holmes *et al.*, 2015), all of which are stratigraphically above, and largely spatially to the south of Sea Lion (Fig. 2). The Casper and Beverley fans have been described (see Bunt, 2015; Francis *et al.*, 2015; Williams, 2015), with the style of deposition for Casper and Beverley attributed to 'mass flows' or 'liquefied sediment gravity flows' (*sensu* Lowe, 1982), comprising 'ungraded, structureless sand' (Williams, 2015). The plan-view distribution and seismic character of the Beverley Fan is displayed in Francis *et al.* (2015) and Lopez Marmolejo *et al.* (2018). The Zebedee Fan is briefly discussed in Davis *et al.* (2018), where six 'facies' were recognized within open-hole log data.

METHODS AND DATASETS

Geophysical interpretation

In order to constrain fan geometries in 3D space, this study uses >4500 km^2 of 3D seismic reflectivity data from multiple surveys collected across the NFB, acquired between 2007 and 2011. The surveys were merged into a single seismic volume in 2012. This merged full-stack 3D volume has undergone Kirchoff pre-stack time migration and spectral broadening. The polarity of these data is zero phase European (SEG reversed polarity). The vertical limit of resolution of the seismic data, at the interval of interest, is *ca* 15 m.

Individual fans and internal lobes were mapped on seismic sections within the 3D volume. From this mapping, a series of seismic reflection amplitude extraction maps were made. Amplitude maps were created by extracting average seismic amplitudes from a ±10 msec window around the mapped horizon. The resultant extractions were plotted as a colour display, with bright colours representing high response, and dark colours indicating low seismic response. From these maps, a range of intra-fan-scale or intra-lobe-scale seismo-geomorphological architectures were identified. These seismo-geomorphological architectures were qualitatively assessed in terms of sedimentary processes of emplacement. Where possible, and for consistency with previous depositional models for deep-lacustrine systems, terminology for these features is applied in-line with Dodd *et al.* (2019). Wireline data from a series of wells (14/10-8; 14/10-9 and 14/10-9Z; 14/15-4 and 14/15-4Z; 14/15b-5; 14/15-2; and 14/15-3), which intersect the interpreted fan systems, have been used to locate the position of cored intervals and for correlation.

Variations in amplitude are directly related to depositional trends and to bulk lithological variations. However, some amplitude responses may be related to the effect of variable fluid fill (for example, hydrocarbons versus water), and thin-bed seismic tuning effects (e.g. Simm & Bacon, 2014; for details see Francis *et al.*, 2015). Aspect ratios were calculated as the maximum length (km) divided by the maximum width (km).

Sedimentological analysis

This study analyses 100 m of core recovered from three wells (14/10-9Z, 14/15-4Z and 14/15b-5): 1:10 cm scale sedimentological logging

was completed to capture information on grain size, lithology and sedimentary structures. All depths are recorded in measured depth below rig table (MDBRT). These data and interpretations are supported by high-quality core photographs of key intervals. A total of 17 facies are recognized (Tables 1 and 2) and grouped into either bed types or facies associations. Wireline data has been evaluated for lithological information of non-cored intervals, but mainly to place cored-sections in stratigraphical context. The results of the sedimentary facies analysis were compared with seismo-geomorphological observations of the three fans to validate the seismic-based interpretations. Through this approach, the character of the deep-lacustrine fans and internal sedimentology is explored.

THREE-DIMENSIONAL SEISMIC AND WELL DATA INTERPRETATION

The Casper Fan System

The Casper Fan System ('Casper') is composed of two lobes: the younger Casper 10 lobe (CA10) and older Casper 20 lobe (CA20), which show some degree of compensational stacking along their margins (Fig. 5). Sediment was fed to the Casper Fan through a feeder system located to the south-east of the Sea Lion Fan, sharing the same entry point as the older Otter Fan (Fig. 2B; *sensu* Dodd *et al.*, 2019).

Casper has an elongate geometry (aspect ratio of 4), with CA10 being *ca* 9 km in length and *ca* 3 km in width, and CA20 reaching *ca* 13 km in length and *ca* 2.5 km in width. Casper is fed through a broad feeder channel (*ca* 600 m wide), which branches outward into a series of intra-lobe features. The zone between the head of the mapped feeder and fan branching displays comparably dimmer seismic amplitudes than the more lobe-dominated parts of the system (Fig. 5A), which may suggest contrasting sedimentology and thickness variation. This area is interpreted as its 'channel to lobe transition zone' (CLTZ, Fig. 5; Mutti & Normark, 1987; Wynn *et al.*, 2002; Brooks *et al.*, 2018). The CLTZs represent areas of sediment by-pass, erosion, coarser grained deposition and soft-sediment deformation (Brooks *et al.*, 2018).

Sinuous seismic architectures are dominant in CA10, whilst anastomosing geometries feature in CA20 (Fig. 5). Areas of comparably low seismic amplitude exist between the sinuous and anastomosing geometries. In both lobes, the constriction of Lobe Axis FA belts (or 'flow constriction' of Dodd *et al.*, 2019) is observed relative to the up-dip areas where the lobe axis is otherwise more widely distributed, with subsequent down-flow widening of geometries in distal areas, forming terminal mouth lobes (Fig. 5).

Using these observations, and comparisons with analogous studies (Dodd *et al.*, 2019), the sinuous and anastomosing seismic geometries likely reflect relative sandstone and non-sandstone distribution, and are therefore interpreted as sinuous and anastomosing lobe axis deposits. Lower seismic amplitudes between these features are interpreted as stranded lobe fringe areas, representing relatively-axial and typically medial areas comprised of lower-energy lobe fringe deposits (*sensu* Dodd *et al.*, 2019). The constriction of seismic architectures reflect areas where flows were focussed into palaeo-topographical lows, by-pass zones across the fan surface or channel exits. Associated down-flow widening features in distal areas have previously been observed in the Sea Lion Fan, and interpreted as terminal mouth lobes (*sensu* Dodd *et al.*, 2019). These are regarded as similar to 'frontal splays' described elsewhere (Cronin *et al.*, 2018).

Three wells intersect Casper (14/10-8; 14/10-9 and 14/15-4), with core in two side-tracks (14/10-9Z; 14/15-4Z); core was not recovered from 14/10-8 (Fig. 4). Core from 14/10-9Z intersects CA10 in an area of sinuous lobe axis deposits. This particular location represents a transitional zone from the lobe axis to a terminal mouth lobe area, in a possible channel exit location (Fig. 5A). 14/15-4Z intersects CA20 in a distal, lobe fringe area (Fig. 5B).

The Zebedee Fan

The Zebedee Fan ('Zebedee') is a single entity at seismic resolution (i.e. no imaged internal lobes; Fig. 6). From relative stratal relationships, Zebedee is younger than Casper, entering the basin from a south-easterly located feeder channel (Figs 2B and 3).

Zebedee forms a branching-outward geometry in its proximal to medial areas, transitioning into a finger-like system distally (Fig. 6). In the proximal areas, Zebedee's feeder channel is east–west oriented, which swings north-east/south-west, and then fans-out distally in a broadly ENE–WSW direction. In the proximal areas, the feeder channel is *ca* 750 m wide,

broadening to *ca* 4 km, before bifurcating in the medial parts of the fan. Zebedee's south-eastern extent has a linear edge, which is in contrast to the rest of the fan where the margins are otherwise lobate (Fig. 6B). Internal features include seismically-bright anastomosing seismic architectures, with areas of comparatively low seismic amplitude response in between. Down-flow widening is prevalent in northerly and westerly areas of the distal fan, but otherwise the system ends as a series of 'finger-like' terminations, with seismic amplitudes diminishing towards the fan pinch-outs.

At the fan scale, the changes in flow direction in the proximal part of Zebedee (Fig. 6B) indicate palaeo-topography influenced overall fan architecture. Similarly, the linear south-eastern margin suggests a component of lateral confinement, possibly by an along-strike-located adjacent slope. The seismically-bright anastomosing seismic architectures likely reflect relative sand distribution and are interpreted as anastomosing lobe axis deposits. Areas of low amplitude represent stranded lobe fringe areas, reflecting inter-flow zones across the fans' surface. It is possible that these areas represent a form of flow-scale relief (*ca* >1 m to <10 m relief), with which flows interacted, ultimately as a function of autogenic compensational stacking (*sensu* Prélat *et al.*, 2009; Spychala *et al.*, 2017a,b). The examples of down-flow widening are associated with development of terminal mouth lobes in the distal-most part of the fans (*sensu* Dodd *et al.*, 2019).

Zebedee is intersected in three wells: 14/15-2, 14/15-3 and 14/15b-5, with the latter cored (Figs 4 and 6). Well 14/15b-5's exploration target was the Zebedee Fan, through which *ca* 45 m of core was collected from a stranded lobe fringe area (Figs 4 and 6A).

The Beverley Fan System

The Beverley Fan System ('Beverley'; Fig. 7) is younger than Casper and Zebedee (Figs 2B and 3), and is composed of two lobes: the younger Beverley 10 (BEV10) and older Beverley 20 (BEV20). Beverley feeds into the basin from a location to the south-east of the Casper and Zebedee feeder systems (Fig. 2B).

The fan system is elongate (aspect ratio of 2.7), with BEV10 reaching *ca* 15 km in length and *ca* 3.5 km in width, and BEV20 *ca* 15 km in length and *ca* 6 km in width (Fig. 7A). The two lobes are largely offset, that is other than

minor coalescing in the medial and distal fan (inset, Fig. 7A). Beverley was fed by a narrow (*ca* 200–300 m wide) straight feeder channel that bifurcates into a number of weakly sinuous geometries downstream. The zone between the head of the feeder channel, and the point of bifurcation, displays a seismically dimmer response than the more lobe-dominated parts of the system.

In the distal areas, the seismic amplitude architectures (Fig. 7A) comprise largely narrow (typically 100–250 m wide), linear to weakly sinuous geometries, aligned parallel to the elongation-strike of the fan system. Low amplitude areas separate the sinuous and linear geometries, especially in the medial parts of the fan. Distal areas are characterized by a transition from linear or sinuous geometries, into down-flow widening architectures that form approaching abrupt fan pinch-outs.

The weakly sinuous to linear architectures are interpreted as sinuous and linear lobe axis deposits, which form the main sediment conduits to the more distal parts of the fan. Down-flow-widening features are interpreted as terminal mouth lobes (*sensu* Dodd *et al.*, 2019), and may have formed through by-pass of more proximal areas during fan growth. Alternatively, these features may have formed as a result of local changes in slope profile, causing the transition from lobate deposits in proximal to medial areas, narrowing to linear channel features as slope gradient increased, then transition to terminal mouth lobe features as the slope profile shallowed. The coalescing of BEV10 and BEV20 in the distal parts of the fan system might suggest the influence of palaeo-bathymetry on the loci of the terminal mouth lobes (see Fig. 7A).

The elongate nature of Beverley, and narrow largely linear lobe axis geometries that characterize the fan, represent a contrasting system compared with older fans within LC3 (i.e. Casper and Zebedee; Sea Lion, see Dodd *et al.*, 2019). The fan has a contrasting overall flow direction, with older fans taking a broadly northeast/south-west path, whilst Beverley has a dominant ENE–WSW strike (Fig. 2B). Like the Casper and Zebedee fans, the low amplitude areas in the proximal-most part of the fan are interpreted as a CLTZ. As Beverley represents a slightly younger fan system, entering the basin during a time when fluvial influence (input) is inferred to have been enhanced (Holmes *et al.*, 2015), it is possible that the more elongate profiles and fan orientation are related to increased

fluvial drainage in upper LC3. Finally, the influence of variable palaeotopography is thought to have had at least some control upon the overall distribution of Beverley.

Beverley is drilled in two wells (14/15-4 and 14/15b-5), one of which is side-tracked and cored (14/15-4Z), intersecting BEV10 (Fig. 4) in a terminal mouth lobe area (Fig. 7B).

FACIES ANALYSIS

Of the 17 identified facies, eight characterize the HEBs, at the 'bed type' scale (Table 1), whilst nine facies make-up key reservoir components of the coarse-grained deep-lacustrine fan model (Table 2) and are grouped at facies association level. Through this approach of first characterizing HEB bed types, and then analysing facies associations of the sedimentary environment, HEBs are placed within spatial and temporal context of the coarse-grained deep-lacustrine fan model.

Facies analysis part I: Hybrid Event Beds (a bed type)

In order to sub-divide the HEBs, this study applies the 'H' nomenclature of Haughton *et al.* (2009), which is widely used (e.g. Pierce *et al.*, 2018; Hussain *et al.*, 2020), where HEBs are divided into five principal units (H1–H5) (Fig. 1). Detailed descriptions and distinguishing criteria are provided in the HEB facies scheme of Table 1, whilst example images are provided in Figs 8 to 11. Interpreted sedimentary processes for the emplacement of each unit and sub-unit are provided below. The subdivision of H1 (i.e. H1a and H1b) follows that proposed by Pierce *et al.* (2018), and the bi-partite subdivision of H3 (i.e. H3a and H3b) of Hussain *et al.* (2020) is amended to permit the incorporation of a third sub-unit identified in this study (H3c).

Units H1a and H1b Interpretation
H1a is interpreted as deposition under a high-density turbidity current that was non-cohesive, with high suspension fall-out rates, forming the thickly-bedded structureless sandstones (Fig. 1B; Lowe, 1982; Haughton *et al.*, 2009; Southern, *et al.*, 2017).

H1b is more variable in its transport mechanisms than H1a. Examples where normal grading is present suggest vertical bed aggradation and deposition from less-energetic and decelerating non-cohesive flows. The thin ripple-cross and parallel laminations at the top of the unit support sedimentation under traction, perhaps under more dilute turbulent conditions in the tail of a rapidly-decelerating high-density turbidity current. In other examples, lofted or rafted mud-clasts near to the top of the unit capture vertical (and/or longitudinal) sorting (Figs 9D, 10B and 11B), attributable to turbulent lift and buoyancy processes (Postma *et al.*, 1988); this is thought to be common for high-density turbidity currents where granular support is typically high (see Lowe, 1979). The absence of fluid escape features and the transitional boundary with underlying H1a units permits the interpretation of high-density turbidites.

For units of H1b, the erosion of muddy substrate, and subsequent lofting plus disaggregation of mud-clasts within flows is interpreted to have increased cohesion, potentially affecting flow velocity. Substrate de-lamination (*sensu* Fonnesu *et al.*, 2016) in up-dip parts of Casper, Zebedee and Beverley likely sourced the muddy material, contributing to erosional bulking. In addition to up-dip erosion, the initial mud-prone substrate of the lake floor, across which early flows travelled, would have allowed for simple and efficient contribution of mud to initially more-turbulent flows, promoting mixed flow behaviour in the early parts of the fan system.

Unit H2 Interpretation
H2 is interpreted as the product of unstable flow conditions (unsteady state or transitional flow; Fig. 1B), with non-cohesive flow and rapid suspension fall-out fluctuating with more-dilute turbulent conditions (Haughton *et al.*, 2009). The banded textures observed in H2 have been interpreted as a range of bedforms formed within the upper-stage plane-bed regime, related to traction beneath a mud-laden transitional plug flow (Stevenson *et al.*, 2020). H2 is rare in this dataset, which may simply reflect a lack of preservation, facilitated through either non-deposition or erosion between the turbulent head and the trailing H3 debris flow (see below); it is common for H2 to be absent (see Haughton *et al.*, 2009).

Unit H3 Interpretation
In this study H3, and its three internal subdivisions (H3a, H3b and H3c; Table 1), are interpreted as the product of a series of separate flow components, which display varying degrees of cohesion, strength and (quasi)laminar flow properties (Fig. 1B; debris flows; *sensu* Lowe, 1982). The key evidence for three separate flow

Table 1. The hybrid event bed facies scheme of this study. Hybrid event beds are divided into eight 'facies' or 'sub-units', including: H1a, H1b, H2, H3a, H3b, H3C, H4 and H5. These subdivisions are all made based on the following criteria (in order of importance): sharp, erosional or loaded contacts; mud-matrix composition (abrupt increases); and sedimentary composition/texture.

Unit title	Unit description	Sub-unit title	Sub-unit description
H1	H1 is divisible into 'H1a' and 'H1b' (Fig. 1; Table 1), often with a transitional boundary between the two units; the contact can sometimes be abrupt, loaded or foundered.	**H1a**	Comprises predominantly clean, structureless, very fine to fine-grained, sometimes medium or coarse-grained, well-sorted, sub-angular to sub-rounded, quartz-rich sandstone (Fig. 8B and C). Rare 1–5 mm wide mudstone flakes can be present in the matrix. H1a often displays an erosional base with the underlying unit (substrate), which can comprise either hemi-limnic mudstones (Fig. 9B and C), turbiditic sandstones, or preceding HEBs (Figs 10E and 11D); bed bases are loaded/foundered in places (e.g. Fig. 11B).
		H1b	H1b comprises structureless fine to coarse-grained, well-sorted, sub-angular to sub-rounded, quartz-rich sandstone, which is often finer-grained than its associated H1a unit (where present). H1b's lower contact is typically gradational. Dispersed carbonaceous clasts, extraformational clasts, mud-clasts and an elevated mud-matrix component are typically present (Figs 10B and 11C). Clasts display an upward increase in both abundance and size, sometimes accompanied by an increase in mud-matrix concentration approaching the overlying unit (Fig. 11B and C). Normal grading, ripple-cross-lamination and parallel lamination can appear near the top. Importantly, H1b lacks clear deformed sand patches, 'primary' fluid escape structures, elutriation pipes and micro sand injections, making it distinctly separate from the quite comparable deposits of H3a. When H1b is present, it tends to be followed by a well-developed H3–H5 succession.
H2	H2 comprises very fine to fine-grained, poor to moderately-sorted sandstones, which display elevated mud content (*ca* 2–15% visually) within the matrix. Rare 1–2 cm long, elongate mud-clasts are present within matrix. Chaotic 'banding' of clean sandstone and light-grey mud-rich sandstone. Dish structures are common, which form otherwise structureless sand-patches, as are poorly-developed often mud-draped asymmetrical ripple cross-lamination and planar lamination (Fig. 14D). H2 displays a transitional boundary with the underlying H1 unit and is, as a bulk unit, generally finer-grained compared with its associated H1.		
H3	H3 comprises comparatively more mud-rich sandstones than H1 or H2, is typically mud-clast-rich, and texturally diverse. H3 basal contacts are typically sharp with H1 or H2, but can display foundering. Sharp intra-H3 contacts and visually-identifiable abrupt changes in (mud) matrix composition, sedimentary structures, clast compositions, and textures (across those contacts) are a feature of the complex unit (e.g. Figs 8–11). Consequently, H3 is divided into three separate sub-units, termed: 'H3a', 'H3b' and 'H3c' (Table 1). In general, the mud-matrix content increases moving from H3a–H3c, with step changes in composition, sedimentary structures, and textures across the abrupt intra H3 boundaries.	**H3a**	H3a comprises very fine to medium-grained, sub-angular to sub-rounded, quartz-rich sandstone, with dispersed mud (*ca* 15–25% visually). There are: common dispersed 0.1–8.0 cm long, 0.1–2.0 cm wide elongate and/or tabular mud-clasts (flattened); poorly-defined sometimes sheared sand patches; fluid escape or elutriation pipes; and typically centimetre-scale (>1 cm in width) injectites (e.g. Figs 8B, 8C, 8E and 9C). Mud-clasts typically exhibit clast-to-clast alignment, and in the sandier examples are inclined, with A-axis' ranging from 20–30° with respect to bedding (Fig. 8C). In comparison, when mud-matrix content is visibly higher, mud-clasts align parallel to bedding (Fig. 8B). In some examples, H3a can also be significantly clast-poor. Mud-matrix content often increases gradually towards upper often sharp and/or loaded contacts (typically with H3b; Fig. 8E). H3a has a sharp, sometimes erosional base with H1a or H1b (Figs 8C, 9B and 9C), is loaded (Fig. 9B) and rarely flat. **Distinguishing criteria:** Clear sandstone-dominated matrix; patches of sandstone with higher dispersed mud content; other than fluid escape pipes, lack sandstone injectites.

Table 1. (continued)

Unit title	Unit description	Sub-unit title	Sub-unit description
		H3b	H3b is composed of very fine to fine-grained sandstone with dispersed mud (*ca* 20–40% visually, which is always visibly higher compared with H3a). Common 0.1–8.0 cm long, 0.1–2.0 cm wide, elongate mud-clasts are present, often oriented with their A-axis parallel to bedding. H3b often contains sheared centimetre-scale (>1 cm in width) injectites and/or very fine grained 'clean' sand patches, which tend to be smaller, but better-defined than compared with H3a (Fig. 9B). Injectites produce centimetre-scale mound-like geometries at the top of the unit, especially where they are retained behind elongate mud-clasts within H3b (Figs 9C and 11A). In other instances the injections 'break through' into the overlying unit. When present, H3b sits above H3a (Figs 8C, 9B, 10C, 10E, 11A and 11B). The basal contact is typically sharp and/or loaded. It can also be erosional, and sometimes displays an angular relationship with the underlying H3a unit (Fig. 10C). H3b is also observed directly above H1a or H1b (Fig. 8A and D), with H3a absent in those examples.
			Distinguishing criteria: Matrix is always a mixture of sand patches, mud patches and mud-clasts. Clear sandstone injectites.
		H3c	H3c can be regarded as a mud-rich (dispersed mud *ca* 40–70% visually) and clast-rich sandstone, although it is challenging to accurately discriminate its lithology without thin section analysis. The overall character is a light to medium grey sand/mud matrix, with dispersed thin (*ca* 0.1–0.5 cm wide) elongate dark grey to black mud-clasts carbonaceous clasts and extra-formational clasts, which display strong A-axis-alignment texture (Figs 8–11). Clasts are always dispersed (or suspended) in the matrix and unsorted. Much larger (1–8 cm long, 1–2 cm thick) mud-clasts, and typically-spherical siderite clasts, are present (e.g. Figs 10E and 11E), which are significantly 'out-sized' in terms of the preserved thickness of H3c sub-unit, and its bulk grain size (Figs 9C and 11C). The spherical siderite clasts seem to be exclusive to H3c in this dataset (Fig. 11E). Common out-sized extraformational (Fig. 9A) and carbonaceous clasts (Fig. 10B) are present. The basal contact is always sharp, and often highly irregular with the underlying H3a and H3b (if present; Figs 9A, 10B and 11E). These irregular bases are often erosional (Figs 8B, 8D and 11B). In examples where H3c overlies H3a, H3c has a sharp basal contact, compensationally filling and draping centimetre-scale depositional topography formed by the underlying H3a unit (Fig. 9C), and is locally erosional or angular (Fig. 11B, C and E). When H3c overlies H1a or H1b, the base is sharp and shows evidence for erosion (Figs 8D, 9A and 10E). Injectites, composed of very fine-grained clean sand, are sometimes present in H3c, where they are generally thinner than in H3a and H3b (typically <1 cm in width in H3c). The H3c injectites are more common near the base of H3c and are often 'sheared', parallel to bedding (Fig. 9B).
			Distinguishing criteria: High mud-content; dispersed sand grains; concentrations of carbonaceous clasts that are often dispersed/suspended and often out-sized; strong A axis clast alignment. Clear sandstone injectites; overall medium grey colour.
H4	H4 comprises mudstone and very fine to fine-grained, moderate to poorly-sorted sandstone couplets, often with dispersed sand particles in the muddier layers. H4 displays common parallel lamination, low amplitude ripple cross-lamination, and rare laminae-scale soft-sediment deformation (Figs 8C and 10E). The basal contact of H4 forms as a range of geometries; it is sometimes sharp, and appears to drape clast-scale depositional topography of underlying H3c units (Fig. 10E), is subtly erosional (Figs 8C, 8E and 11C), or quite angular (Fig. 10C).		
H5	H5 comprises dark grey to black mudstone, with common 1–5 mm long elongate mud flakes, carbonaceous flakes and dispersed sand grains in the matrix. Thin very fine-grained sandstone laminae occasionally feature within H5. The basal contact of H5 is either sharp, draping remnant flow-scale topography when overlying H3b (Fig. 8B and D), or is transitional when overlying H3c (Fig. 9B and C).		

Table 2.   Sedimentary facies from the coarse-grained facies model for deep-lacustrine fans. Note, the hybrid event bed facies (of Table 1) are in reality part of this model, but have been placed into separate tables to aid clarity. Nine facies are shown in this table and, together with the eight facies/sub-units of the hybrid event beds, 17 facies in total have been identified within the dataset.

Facies code	Facies title	Facies description	Interpretation
fss	Structureless sandstone	Fine to coarse-grained, well-sorted to very well-sorted, sub-angular, quartz-dominated sandstone. Occasional dark coloured lithic grains are concentrated towards the top of the units. The facies comprise structureless sandstones with loaded bases. Units are found in stacked packages, up to 10 m in thickness, comprising up to 15 amalgamated beds	Rapid suspension fall-out from high density turbidite currents (Lowe, 1982), with enhanced sorting controlled by extensive run-out distances
fnss	Normally-graded structureless sandstone	Fine to coarse-grained, moderate to-well-sorted, sub-angular to sub-rounded sandstone displaying a coarse-grained base, normally grading to fine-grained sandstone in the upper 2–3 cm of the bed. This facies can display thin (<1 cm thick) parallel-laminated, mud-rich bed-tops	Rapid suspension fall-out from high density turbidite current (Lowe, 1982) that was decelerating. The very top of these beds may have been formed within a tractional zone beneath a dilute turbulent flow (Allen, 1984)
fdcs	Dispersed clast-rich sandstone	Poorly sorted, fine to coarse-grained, structureless, sub-angular, clast-rich sandstone. Clasts are composed of a mixture of rounded mud-clasts and sub-angular to sub-rounded lithic fragments. The mud-clasts tend to either be dispersed in the middle-to-upper portion of the bed and are fully-supported by the matrix, or are concentrated towards the top of the bed and sometime show clast-supported textures	Freezing of a high concentration flow, whilst in a laminar state (Mutti & Nilsen, 1981). Deposition of traction carpet (Postma *et al.*, 1988; Sohn, 1997; Cartigny *et al.*, 2013)
fmcs	Mudstone clast-rich sandstone	Fine to medium-grained, well-sorted, sub-angular, structureless sandstone that is mud-clast-rich, and can be either clast-supported or matrix-supported. This facies shares similar qualities to *fss*, with the addition of mud-clasts that tend to be concentrated at the base. Mud-clasts are elongated and range from 2–10 cm long, are sub-angular and are usually composed of mudstone or siltstone. They commonly display lithic grain armouring, indicating partial lithification prior to rip-up, entrainment and deposition. This facies occurs at the base of an event bed, usually resting on an erosional base	Rapid suspension fall-out from high density turbidite currents (Lowe, 1982), with angular, armoured clasts indicating up-dip erosion (Haughton *et al.*, 2003). In the examples of *fmcs* that form at bed bases, above erosional contacts, these can be interpreted as by-pass lags (*sensu* Stevenson *et al.*, 2015)
fpxbs	Planar cross-bedded sandstone	Moderately sorted, fine-grained, occasionally medium-grained planar cross-bedded sandstone. Planar cross-bed sets sometimes display an argillaceous, mud-drape, and often poorly developed	Sustained bedload transport beneath flows with relatively low aggradation rates, which by-pass the slope/shelf (Stevenson *et al.*, 2015, and reference therein)
frxls	Ripple cross-laminated sandstone	Fine to medium grained, ripple cross-laminated sandstone, with darker, sometimes carbonaceous/argillaceous silt-grade material, usually defining the ripple foresets. The thicknesses of this facies ranges from 2–10 cm, occasionally reaching 15 cm	Current ripples formed through traction in a decelerating turbulent flow (Walker, 1965; Allen, 1982; Baas, 2004; Baas *et al.*, 2011)
fpls	Parallel laminated sandstone	Very fine to medium-grained, well-sorted, sub-angular, parallel laminated, normally graded sandstone. The parallel laminations are sometimes highlighted by clay to silt grade material in the matrix	Tractional laminations formed by a waning flow (Allen, 1984)

Table 2. (continued)

Facies code	Facies title	Facies description	Interpretation
fism	Inter-bedded sandstone and mudstone	Inter-bedded sandstones and mudstones. Sandstones are characterized as: very fine-grained, ranging to medium-grained, well-sorted, sub-angular to sub rounded, structureless, occasionally parallel laminated, ripple cross-laminated and thin-bedded. Mudstones tend to be <1 cm thick, homogenous and parallel laminated. Common examples of water escape structures and loading. Bioturbation is rare	Post-depositional 're-working', slumping and churning through bottom-water processes (e.g. bottom-currents/contourites) and rare bioturbation. Thin bedded, parallel laminated and ripple cross-laminated sandstones represent tractional features formed by waning dilute flows (Allen, 1984), reflecting intermittent low-density turbidity currents
fplm	Parallel laminated mudstone	Dark grey to black coloured, homogeneous mud to silt grade, parallel-laminated siliciclastic mudstones. The laminations are depicted by subtle variations in colour and grain size	'Background' hemi-limnic suspension fall-out in the water column (Stow & Tabrez, 1998; Dodd *et al.*, 2019). Laminations represent seasonal variability in lake productivity. Alternatively, at least some of these facies could represent dilute remnants of turbidity currents (*sensu* Boulesteix *et al.*, 2019)

components includes: abrupt breaks, or increases in mud matrix concentrations across sharp boundaries; erosional, angular and loaded contacts; variability in sedimentary composition; clast orientation and alignment; and sheared sand patches. The absence of re-working/bioturbation, or other deposits in between these sub-units, such as hemi-limnic mudstone drapes, suggests that they were deposited as part of the same event bed.

The low mud-matrix concentration of H3a, often with patches of intercalated cleaner sand, suggests remaining fluidization prior to deposition, or that the flows were transitional in rheology. The numerous inclined A-axis aligned elongate dispersed mud-clasts suggest at least some component of laminar flow and shear, and possible development of non-deforming plug flow (*sensu* Sohn *et al.*, 2002). The lack of ripples and other bedforms might suggest deposition under upper transitional plug flow conditions (*sensu* Baas *et al.*, 2009, 2011). The loaded bases indicate that H3a was deposited on top of a still fluid-rich H1a/H1b unit, through which it was able to sink (for example, Fig. 9).

The higher mud-matrix content and textural variability of H3b (compared with H3a), along with the sharp and sometimes erosional contacts with H3a, indicates a separate flow component, with different rheological properties (for example, Fig. 8E). The successive relationship of H3a and H3b within a single event bed (for example, Figs 8E and 9B) demonstrates the presence of two penecontemporaneous units. The higher mud-matrix content, mud-clasts and isolated sheared sand patches suggest a flow that had reduced, but still moderate shear strength in comparison with H3a. The lack of ripples suggests that deposition occurred under upper transitional plug flow conditions (*sensu* Baas *et al.*, 2009, 2011), but perhaps at a different stage of flow transformation than compared with H3a.

Collectively, the bed-parallel shear textures (Figs 9B, 9C and 11A), imposed upward mounding of the top H3b surfaces by intruding injectites associated with H3c emplacement (for example, Fig. 9B), and varied expression of H3c's sharp, loaded, and erosional or angular basal contacts (for example, Fig. 10C) with H3a or H3b, indicate that H3c is the product of a discrete flow component. The high mud-matrix content and strong A-axis-bedding-parallel clast alignment suggests a low-strength, (quasi)laminar plug flow (*sensu*
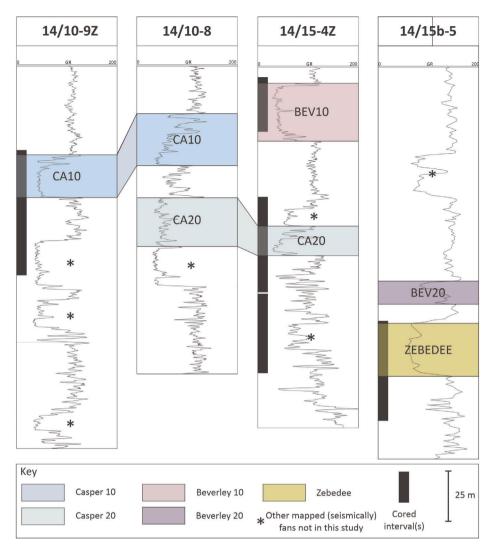
Fig. 4. Wireline logs from wells drilled through the three fans in this study. Gamma Ray (GR) data is provided, showing low values to the left (sandier) and higher values to the right (muddier). The position of the core points within the available well dataset that intersect the three fans is provided (black boxes). Fan system/lobe geobodies are marked, with fan bases/tops interpreted from seismic interpretations data, and checked based on well response (i.e. aligned with nearest sandstone bases). Wells have been correlated where possible *(BGS © UKRI 2022)*.

Baas *et al.*, 2009; Talling, 2013). The large carbonaceous clasts, extraformational clasts and siderite, which are often significantly out-sized compared with the rest of H3c, suggest that these flows retained some strength in order to suspend the large, perhaps comparatively more-buoyant, clasts (*sensu* Pierson, 1981), in the mud-rich flow. Considering H3 as a whole, it would seem challenging to produce most of these characteristics by vertical stratification, where settling processes form interfaces between H3 sub-units (see also Hussain *et al.*, 2020).

This study interprets the presence of at least three separate sub-units within H3, all of which being deposited by different flow components during a single flow event (Fig. 12). Each flow component had different rheological properties and flow characteristics. Sharp, erosional, angular and loaded intra-H3 contacts provide evidence for at least some temporal spacing between the emplacement of H3a, H3b and H3c. The erosional contacts suggest that at least the head of each flow component was eroding substrate, and entraining material from previous H3 deposits.
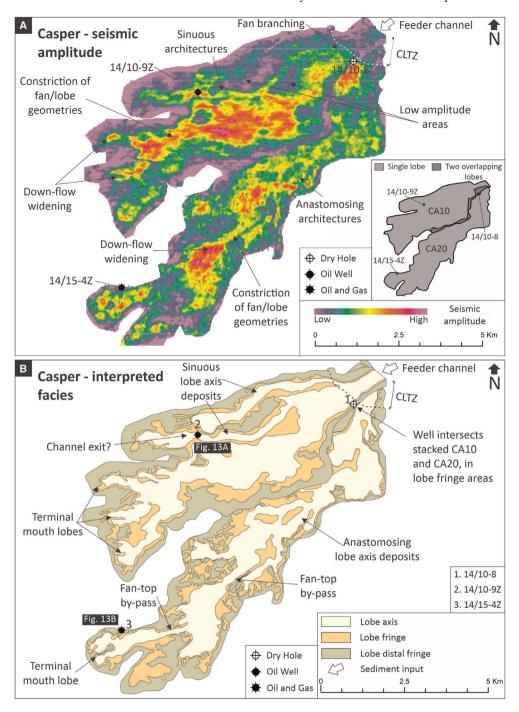
Fig. 5. The seismic character and interpreted facies of the Casper Fan. (A) Seismic amplitude maps of the Casper Fan. The Casper Fan is composed of two lobes, termed CA10 and CA20 (see inset map). A range of internal seismic architectures can be observed from different parts of the fan (see labelled arrows). (B) Interpreted facies maps from the Casper Fan. Three wells intersect Casper, 14/10-8, 14/10-9 and 14/15-4. Core exists from the lobe axis in 14/10-9 (see Fig. 13A), and the lobe fringe in 14/15-4 (see Fig. 13B) (*BGS © UKRI 2022*).

Unit H4 Interpretation

H4 is interpreted as tractional structures formed by flows in the dilute turbulent wake during unsteady-state flow (*sensu* Haughton *et al.,* 2009). The irregular nature of the H4 basal contact is attributed to either erosion of H3 deposits by these more-dilute flows, loading of H4 sands into fluid-rich muddy H3 (*sensu* Fonnesu
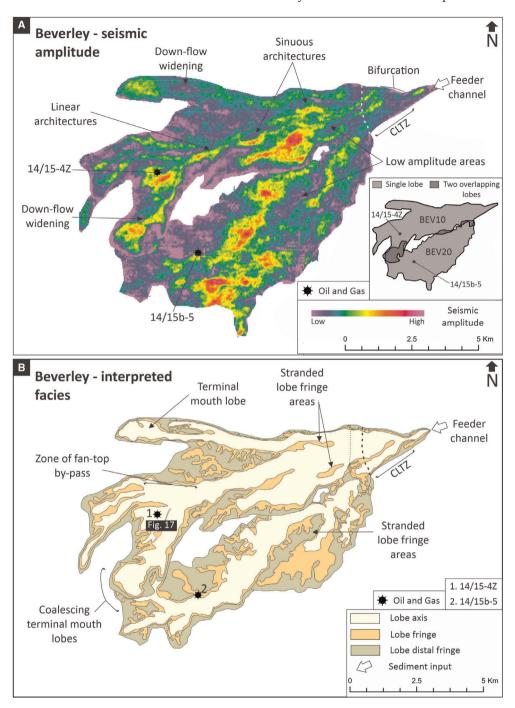
Fig. 6. The planform seismic character and interpreted facies of the Zebedee Fan. (A) Seismic amplitude maps of the Zebedee Fan. (B) Interpreted facies maps from the Zebedee Fan *(BGS © UKRI 2022)*.

et al., 2015), or the draping of H3-surface topography.

Unit H5 Interpretation

H5 is interpreted as suspension fall-out within a perturbed water column. Micro mud-clasts and carbonaceous matter are commonly left suspended after the flows have passed, which later vertically aggrade. As these particles settle, the lake floor sediments gradually transition back into normal background sedimentation processes. Following HEB deposition, successive mixed flows were able to modify or even re-

Fig. 7. The planform seismic character and interpreted facies of the Beverley Fan. (A) Seismic amplitude maps of the Beverley Fan. (B) Interpreted facies maps of the Beverley Fan *(BGS © UKRI 2022)*.

work the previous deposits, indicated by shearing and modification of H3 and H4 units by overriding flows (Fig. 9C), and by erosive contacts between stacked HEBs (for example, Figs 8A and 10E), respectively.

Facies analysis part II: Coarse-grained fan deposits

For the Casper, Zebedee and Beverley Fans, nine facies (Table 2) have been grouped into three

Fig. 8. Example image of core from hybrid event beds from the Casper 10 Lobe (see Fig. 13A for in-core locations). (A) Five stacked hybrid event beds (14/10-9Z, 2435.45 m). (B) Four stacked hybrid event beds (14/10-9Z, 2434.25 m). (C) Two stacked hybrid event beds, with the lower example showing a relatively complete 'H-sequence', other than H2 being absent (14/10-9Z, 2420.00 m). (D) Three stacked hybrid event beds (14/10-9Z, 2417.35 m). (E) Five stacked hybrid event beds (14/10-9Z, 2414.35 m) (*BGS © UKRI 2022*).

'facies associations' (FA), termed: 'Lobe Axis FA', 'Lobe Fringe FA' and 'Hemi-Limnic Mudstones FA' (Figs 13 to 18). Because cored intervals are limited for the three fans (*ca* 100 m across four wells), this dataset does not contain core from more distal parts of the deep-lacustrine fan (for example, the lobe distal fringes). Analogous facies associations in the more distal and lateral part of the deep-lacustrine fan have been documented from the nearby Sea Lion Fan (see Dodd *et al.*, 2019). Consequently, HEB distribution is considered in the context of the lobe axis and lobe fringe areas for this study, although the Sea Lion Fan provides some details for other areas (Dodd *et al.*, 2019).

Lobe Axis Facies Association
Description. The Lobe Axis FA largely comprises fine or medium-grained, and sometimes coarse-grained structureless sandstone (*fss*), with subordinate parallel-laminated sandstone (*fpls*), normally-graded structureless sandstone (*fnss*) and rare planar cross-bedded sandstone (*fpxbs*; Table 2; Figs 13 to 19). *Fss* typically has sharp contacts at the bed base and occasional dish or dewatering structures. *Fnss* is often accompanied by an upward increase in mud-matrix content, signified by darker coloured bed-tops and a reduction in oil staining. Successive beds are typically amalgamated but may be separated by a thin (1–5 cm thick) unit of parallel-laminated mudstones (*fplm*). Individual beds range between 0.25 to 5.0 m in thickness and are encountered in amalgamated packages of up to 8 m in thickness. Facies mud-clast rich sandstone is encountered at or near bed bases (*fmcs*), and dispersed clast-rich sandstone (*fdcs*) is found concentrated towards the top of the bed.
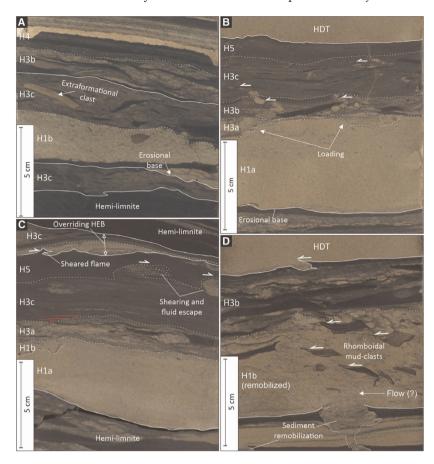
Fig. 9. Example image of core of hybrid event beds from the Casper 20 Lobe (see Fig. 13B for in-core locations). (A) Three stacked hybrid event beds (14/15-4Z, 2441.20 m). (B) A single hybrid event bed (14/15-4Z). (C) Two stacked hybrid event beds (14/15-4Z, 2440.15 m). (D) A single hybrid event bed, with an underlying sediment remobilization feature (14/15-4Z, 2439.75 m) *(BGS © UKRI 2022).*

Interpretation. The Lobe Axis FA was formed by high-density turbidity currents that deposited thick typically amalgamated structureless fine or medium-grained sandstones (*fss*). High-sediment concentrations in the flow led to near-bed turbulence suppression, such that tractional sedimentary structures (*fpls*) are subordinate (Lowe, 1982; Sumner *et al.*, 2008). Dewatering structures preserved in *fss* are interpreted as deposition from more-fluidized versions of flows. Amalgamated beds of *fss* represent erosion by subsequent flows. This leads to stacked units of structureless sandstone that are the product of multiple flow events, which reflects a relatively high energy location typical of the lobe axis (*sensu* Prélat *et al.*, 2009). Intervals of *fmcs* and/or *fpxbs* are interpreted as reflecting sediment by-pass (*sensu* Stevenson *et al.*, 2015). Beds of *fdcs*, particularly when preceded by *fnss*, are interpreted to reflect traction carpet sedimentation (Postma *et al.*, 1988; Sohn, 1997; Cartigny *et al.*, 2013), which are texturally similar to D3 beds of Hodgson (2009). Preserved units of *fplm* represent the product of either temporary breaks in fan

activity or lobe switching (*sensu* Burgess *et al.*, 2019).

Lobe Fringe Facies Association
Description. The Lobe Fringe FA consists primarily of sandstone-prone facies, including well-sorted *fss,* ripple cross-laminated sandstone (*frxls*), *fpls* and common *fnss*. Inter-bedded sandstone and mudstone (*fism*) and parallel-laminated mudstone (*fplm)* also feature, but to a lesser-extent (Table 2; Figs 13 to 19). Units of *fss* are rarely amalgamated, and are typically separated by 1 to 50 cm thick beds of *fplm* or *fism*. Individual event beds tend to be thin (0.01 to 1.0 m thick), and more commonly comprise *fnss*, with subordinate *fss*, often with well-developed *frxls* and/or *fpls* at the bed tops. HEB bed types are observed within the Lobe Fringe FA.

Interpretation. The Lobe Fringe FA is interpreted to be the product of a mixture of high-density turbidity currents (high-density turbidites; *fss* capped by *frxls* and/or *fpls*) and low-density turbulent flows (low-density turbidites; *fpls* and/
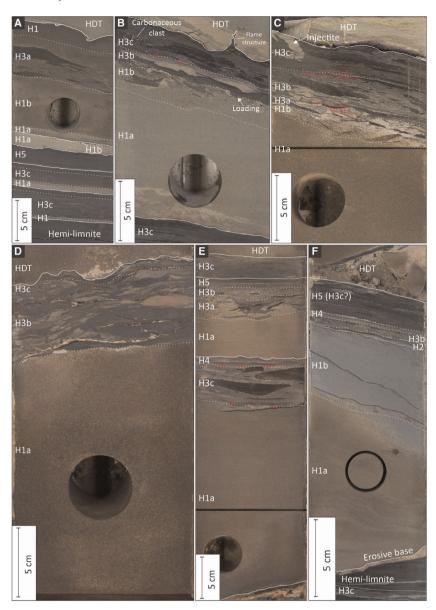
Fig. 10. Example image of core of hybrid event beds from the Zebedee Fan (see Fig. 15 for in-core locations). (A) Four stacked hybrid event beds (14/15b-5, 2484.10 m). (B) A single hybrid event bed, displaying a H1a unit, overlain by H3a and H3b, both with sharp, loaded bases, and a H3c unit with carbonaceous clasts and mud-clasts (14/15b-5, 2483.15 m). (C) A single hybrid event bed with angular contacts between the H-sequence sub-units (14/15b-5, 2482.00 m). (D) A single hybrid event bed (14/15b-5, 2479.50 m). (E) Three stacked hybrid event beds (14/15b-5, 2467.15 m). (F) A single hybrid event bed (14/15b-5, 2456.40 m; *BGS © UKRI 2022*).

or *frxls*). In this study, the Lobe Fringe FA includes elements of both the 'Lobe off-axis' and 'Lobe fringe', as identified in previous studies (see Prélat *et al.*, 2009). In the example of high-density turbidites deposited in the Lobe Fringe FA, the lack of dewatering structures that would otherwise indicate near-bed turbulence suppression and *en-masse* deposition, along with common normal grading, suggests that deposition occurred beneath decelerating flows. The repeated occurrences of interbedded *fism* or *fplm* are interpreted as regular and substantial periods of inactivity in these locations. However, the possibility for at least some instances of *fism* or *fplm* relating more to dilute distal deposits of adjacent flows (*sensu* Boulesteix *et al.*, 2019) is not discounted.

Hemi-Limnic Mudstones Facies Association

Description. The Hemi-Limnic Mudstones FA is comprised of *fplm* intervals that are typically >1 m thick. The *fplm* is composed of laminae-scale alternations of slightly thicker mud-grade material and thinner silt-grade laminae (Table 2; Figs 13 to 19). They contain little evidence for bioturbation and are otherwise homogeneous, except for occasional 1 to 10 cm thick, light-grey to orange, siliceous bands of clay-grade material and common centimetre-scale injectites (for example, above Zebedee in Fig. 15). For units of laminated mudstones <1 m in thickness, these deposits remain classified at the facies level (as *fplm*). Occasional thin-bedded (<10 cm thick) *fpls*, *frxls* or isolated HEBs also
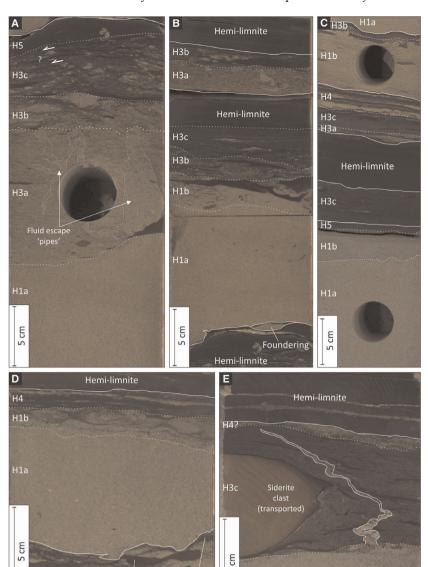
Fig. 11. Example image of core of hybrid event beds from the Beverley Fan (see Fig. 17 for in-core locations). (A) A single hybrid event bed (14/15-4Z, 2381.80 m). (B) Two hybrid event beds separated by hemi-limnite (14/15-4Z, 2381.50 m). (C) Hybrid event beds, hemi-limnite, followed by two stacked hybrid event beds (14/15-4Z, 2369.80 m). (D) A hybrid event bed overlying a mud-clast-rich surface, displaying a micro-rugose texture (14/15-4Z, 2365.00 m). (E) A single hybrid event bed showing well-developed H3c that contains a large, outsized clast that has been replaced by siderite (14/15-4Z, 2358.20 m; *BGS © UKRI 2022).*

feature, most typically, immediately beneath fan systems.

Interpretation. These deposits represent the background hemi-limnic sedimentation of the lacustrine environment, with seasonal variations in productivity forming the laminations (Anderson & Dean, 1988). Deposition occurred through a combination of settling and slow lateral advection (*sensu* Stow & Tabrez, 1998) and was therefore relatively widespread in a basin. Consequently, the relatively gentle and constant deposition of hemi-limnic mudstones can be used as an indication of the general activity or inactivity of each fan and lobe. Thin units of preserved *fplm* represent more temporary breaks in fan activity or lobe switching, and seem to be part of a progressive abandonment phase. Significantly thicker units of mudstone, representing the Hemi-Limnic Mudstone FA (>1 m thick; similar scale to interlobe mudstones of Prélat *et al.*, 2009), reflect major regional breaks in coarser-grained clastic deposition, typically linked to termination.

Heterogeneities, such as units of *frxls* and *fpls* within the Hemi-Limnic Mudstones FA represent low-density turbidites, which may have been isolated flow events, or simply reflect the distal expression of adjacent active fans (*sensu* Boulesteix *et al.*, 2019, and references therein). The siliceous intervals are interpreted as tonstein bands, deposited by ash-fall into a body of freshwater (*sensu* Spears, 2012). The centimetre-scale
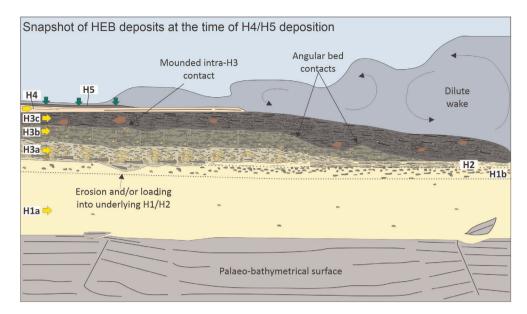
Fig. 12. Schematic model of hybrid event bed emplacement, with particular attention to the H3a, H3b and H3c sub-units. Yellow arrows denote approximate flow direction; green arrows indicate vertical settling. The model represents a 'snapshot' at the time of H4/H5 deposition, towards the end of hybrid event bed emplacement. It illustrates the character of 'H-sequence' units and sub-units identified in this study, along with their 'inter-H' associations (for example, bed contact relationships), and lateral distributions during the emplacement of a single hybrid event bed *(BGS © UKRI 2022).*

injectites are interpreted as post-depositional, and related to over-pressuring within the fan sandstones, as was discussed in detail by Dodd *et al.* (2020). Hybrid event beds encountered in the Hemi-Limnic Mudstone FA are interpreted as the distal expression of flows in neighbouring active systems.
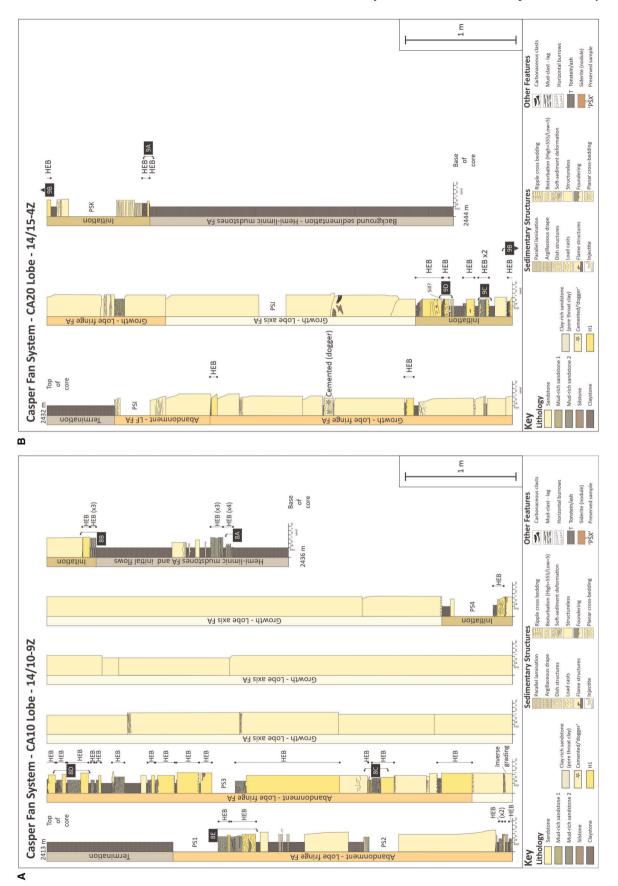
DISCUSSION

Emplacement model for H3 (H3a, H3b and H3c)

The bi-partite sub-division of H3 into H3a and H3b of Hussain *et al.* (2020) discussed two end-member mechanisms for formation, including: 'vertical stratification' through settling of grains during deceleration and eventual arrest leading to deposition of the H3 unit; and 'longitudinal fractionation' where mud is fractionated, both longitudinally and across flows, leading to different 'sectors' with contrasting flow rheologies. The two models are not mutually exclusive, and it is possible for vertically-stratified flows to undergo longitudinal fractionation and transformation (Baas *et al.*, 2011;

Kane & Pontén, 2012; Kane *et al.*, 2017; Hussain *et al.*, 2020). However, the vertical stratification model through settling of grains is thought to not be applicable to those flows that are dense, cohesive and have high mud concentrations (Baas *et al.*, 2011).

This study separates the mud-rich debritic H3 unit into three discrete deposits (H3a, H3b and H3c); despite many similarities, direct correlation between these sub-divisions and those of Hussain *et al.* (2020) is challenging. The sub-units are separated by sharp, erosional or loaded contacts, with visible textural and compositional differences. They document an increase in mud matrix moving from H3a to H3c (Figs 8 to 11). The sharp, erosional or loaded bases, and variations in internal character across those boundaries, indicate discrete flow components within a debris flow responsible for the deposition of the H3 unit. This is particularly interesting, because this is in contrast with the H3 unit often being related to rapid *en-masse* deposition throughout the debris flows length and width. The sharp boundaries, and in particular their erosional (Fig. 10E) or loaded aspects (for example, Fig. 9), along with shearing along bed contacts (Fig. 9B) and high mud-matrix content,

Fig. 13. (A) Sedimentary logs of the Casper 10 Lobe of the Casper Fan System intersected in 14/10-9Z (for well location, see Fig. 5) *(BGS © UKRI 2022)*. (B) Sedimentary logs of the Casper 20 Lobe of the Casper Fan System, intersected in well 14/15-4Z (for well location, see Fig. 5) *(BGS © UKRI 2021)*.
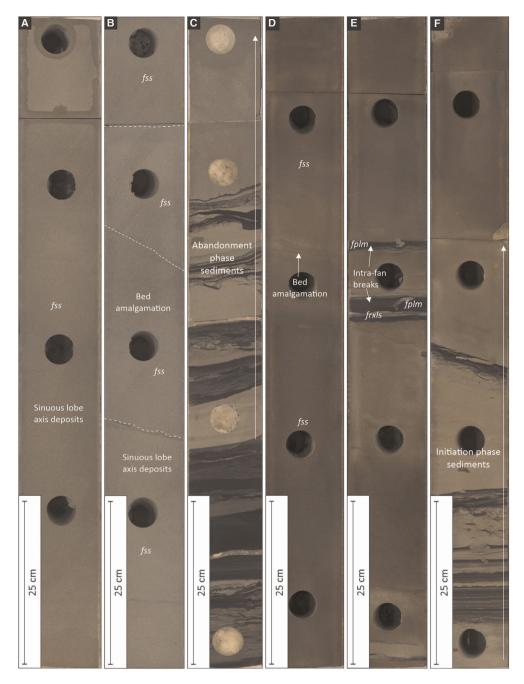
Fig. 14. Examples images of core from the Casper Fan. (A) Example of facies structureless sandstone (*fss*) that characterizes the sinuous lobe axis deposits of the Casper 10 Lobe (top at 2424.87 m, 14/10-9Z). (B) Bed amalgamation of facies structureless sandstone (*fss*) from the Casper 10 Lobe (top at 2420.90 m, 14/10-9Z). (C) Typical core from abandonment successions, example from Casper 20 Lobe (top at 2416.90 m, 14/10-9Z). (D) Facies structureless sandstone (*fss*) and bed amalgamation from the Casper 20 Lobe (top at 2437.00m, 14/15-4Z). (E) Example of intra-fan breaks from the Casper 20 Lobe (top at 2435.00 m, 14/15-4Z). (F) Typical fan start-up succession from the base of the Casper 20 Lobe, with possible banded sandstone (H2) and post-depositional clastic dyke showing some sediment remobilization (top at 2439.00 m, 14/15-4Z) *(BGS © UKRI 2022).*

preclude any model for vertical settling to explain the sub-divisions (Baas *et al.*, 2011; Hussain *et al.*, 2020).

Consequently, this study interprets that H3a, H3b and H3c reflect deposition of a longitudinally-segregated cohesive flow that had
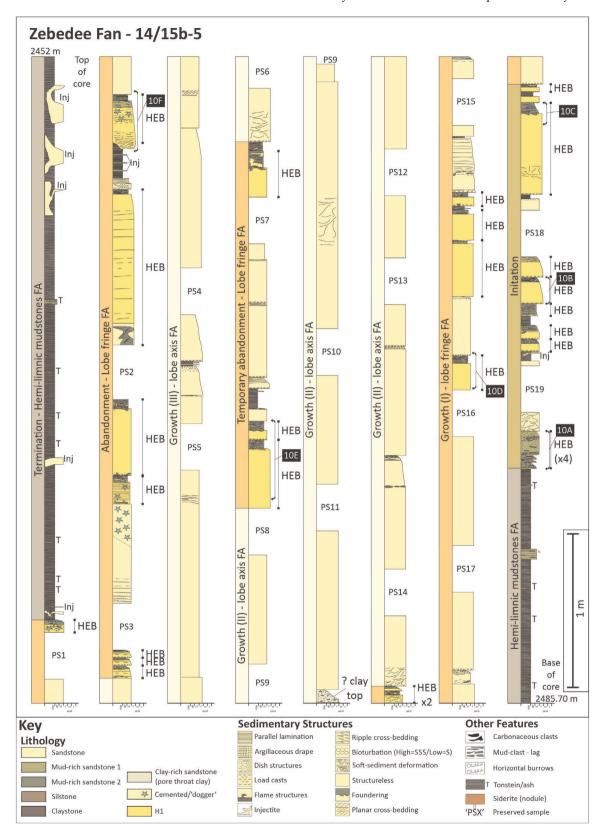
Fig. 15. Sedimentary logs of the Zebedee Fan deposits intersected in well 14/15b-5 (for well location, see Fig. 6) *(BGS © UKRI 2022).*

Fig. 16. Example images of core from the Zebedee Fan. (A) Facies structureless sandstone *(fss)* from the sinuous lobe axis deposits (top at 2471.00 m, 14/15b-5). (B) Example of facies parallel laminated sandstone *(fpls)* and bed contacts (top at 2475.00 m, 14/15b-5). (C) Three separate beds, showing erosional basal contacts (top at 2462.00 m, 14/15b-5). (D) An example of intrafan break overlain by a hybrid event bed (top at 2456.00 m, 14/15b-5). (E) A high-density turbidite with rafted mud-clasts at the top of the bed (top at 2460.00 m, 14/15b-5) *(BGS © UKRI 2022).*

several penecontemporaneous flow components. These formed as a result of advanced rearward longitudinal flow transformation (Haughton *et al.*, 2009; Kane *et al.*, 2017). The idealized H3a–H3c succession (Fig. 1) is sometimes H3a, H3b or H3c absent, which further supports
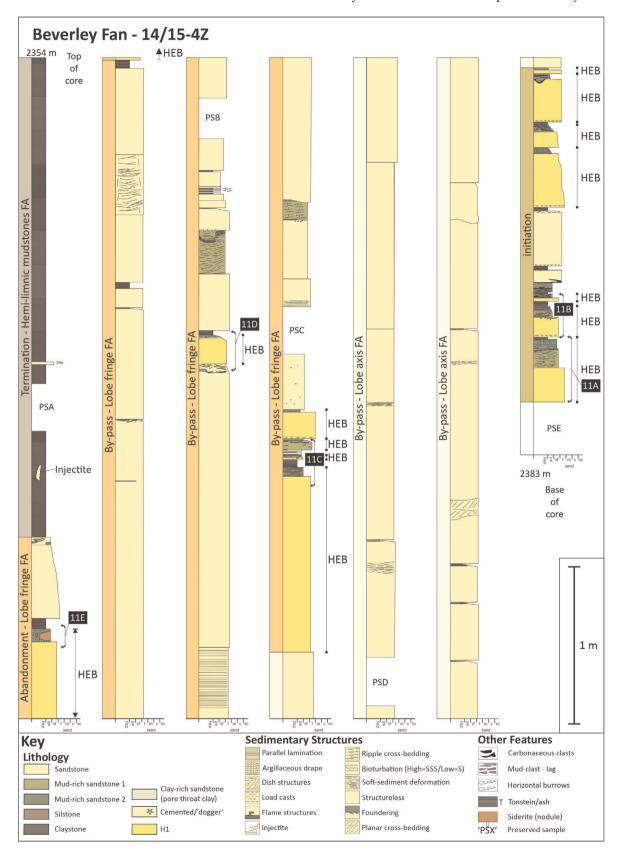
Fig. 17: Sedimentary logs of the Beverley Fan deposits intersected in well 14/15-4Z (for well location, see Fig. 7) *(BGS © UKRI 2022).*

Fig. 18. Example images of core from the Beverley Fan. (A) to (C) Typical examples from the lobe axis deposits in the Beverley Fan [top of (A) at 2366.50 m, 14/15-4Z; top of (B) at 2378.50 m, 14/15-4Z; top of (C) at 2371.50 m, 14/15-4Z]. (D) Examples of high-density turbidites and hybrid event beds (top at 2364.50 m, 14/15-4Z). (E) Examples of intra-fan breaks within the Beverley Fan, dominated by facies parallel laminated mudstones (*fplam*) and thinly-bedded hybrid event beds (top at 2369.50 m, 14/15-4Z). (F) A hybrid event bed at the base of the example, with a large outsized siderite-replaced clast transported and deposited in a H3c unit. The upper part of the core comprises a high-density turbidite that was partially remobilized (top at 2357.50 m, 14/15-4Z). *(BGS © UKRI 2022).*

significant longitudinal complexity of these flows. Entrained mud at the head of the flow became concentrated towards the rear due to inefficient settling, causing the rear of the flows to become more-cohesive and laminar. As the flow became stretched longitudinally, the faster-moving front may have even detached from different parts of the slower-moving tail. Increasing mud content likely influenced, or was influenced by, changes in velocity throughout, and
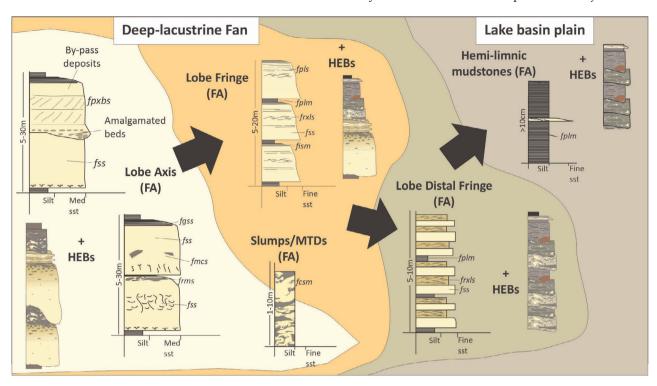
Fig. 19. Idealized facies associations for deep-lacustrine fan systems, based on data from this study, augmented with models from previous studies (after Dodd *et al.*, 2019). The proximal to distal and/or axial to lateral variability in sedimentology depicts decreasing energy and down-flow transition of flows, in terms of both high-density turbidites and hybrid event beds. *(BGS © UKRI 2022).*

along the flows length. These combined factors resulted in segregation into at least three rheologically-contrasting flow components, which deposited H3a–H3c. Baas *et al.* (2021) associated the H3a and H3b units (of Hussain *et al.*, 2020) with "a progressive increase in cohesivity as a result of vertical segregation of the suspended load during deceleration", and the examples provided in the present study contribute to this discussion.

In experimental studies (Baas *et al.*, 2009, 2011), as clay concentration increases, all flows are thought to pass through a predictable set of phases, including: turbulent flow, turbulence-enhanced transitional flow; lower transitional plug flow, upper transitional plug flow and quasi-laminar plug flow. It is possible that H3a–H3c reflect deposition at different points in this transition, namely in the more-cohesive flow phases of upper transitional plug flow and quasi-laminar plug flow, facilitated through advanced rearward longitudinal flow transformation. Whichever phase is represented by H3a–H3c, it is clear from the observations in this study that these sub-divisions are closely related

to sharp changes in mud-content, flow velocity and flow rheology.

Temporal evolution of deep-lacustrine fans

Previous deep-lacustrine fan models have focussed on the spatial evolution (Dodd *et al.*, 2019; Yang *et al.*, 2019; Pan *et al.*, 2020; Shan *et al.*, 2020), with little attention given to their temporal evolution. By contrast, the various stages of initiation, growth and retreat in ancient marine systems have been evaluated by Hodgson *et al.* (2006) and Hodgson, (2009). In order to provide comment on the temporal evolution of deep-lacustrine fan models, this study divides the deposits of Casper, Zebedee and Beverley into six key stages. These include: (T1) Initiation; (T2) Growth (I); (T3) Growth (II); (T4) By-pass; (T5) Abandonment; and (T6) Termination (Fig. 20). During the initiation phase (T1 of Fig. 20), initial flows were small and able to interact with a rugose topography draped with mud and fine-grained sediment, which was readily-available for erosion and entrainment. These deposits reflect the distal-most limits of early flows, and so were
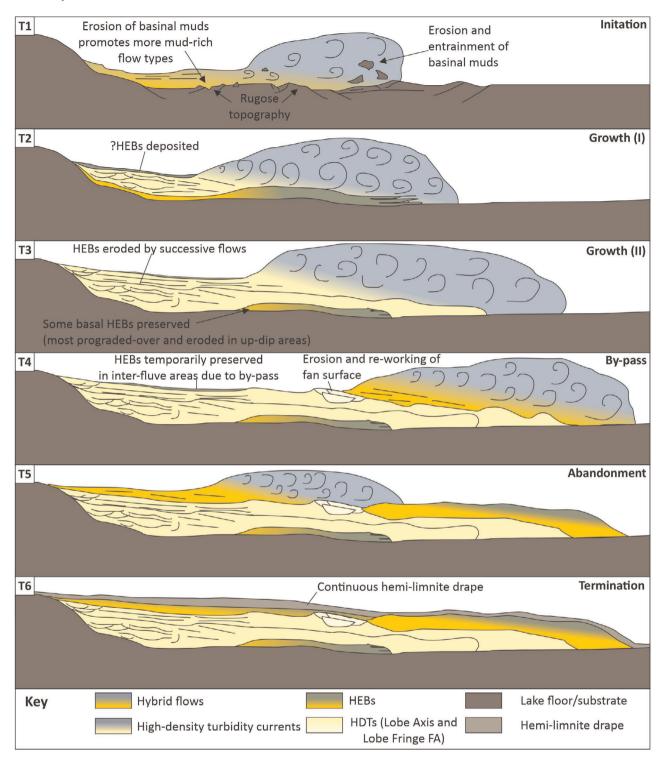
Fig. 20: Temporal-spatial models of potential hybrid event bed occurrence and preserved distribution in the context of deep-lacustrine fan models. (T1) Initiation phase. (T2) Growth phase I. (T3) Growth phase II. (T4) By-pass phase. (T5) Abandonment phase. (T6) Termination phase *(BGS © UKRI 2022).*

later prograded over during the ensuing phases (e.g. Hodgson *et al.*, 2006).

During growth (I), increasingly higher energy sediment-laden flows were supplied to the fan, which began to prograde (T2 of Fig. 20). There was potential for erosion at the heads of these high energy flows, particularly in the proximal and medial, axial parts of the fan. Growth (I) was followed by subsequent phases of development (for example, growth (II); T3 of Fig. 20). Multiple phases of growth is an important consideration in the context of accounting for variable sediment supply and/or lobe-switching (i.e. differential growth within a single fan), and the potential for older deposits of the growth phase (I) to be eroded and re-worked (including HEBs), leading to lower preservation potential.

The by-pass phase (T4 of Fig. 20) reflects periods when large parts of the proximal and medial fan were by-passed, with little-to-no deposition, or erosion, in those areas (Stevenson *et al.*, 2014). Some areas show bed-scale channelling, particularly in the more proximal or axial parts of the fan, where the by-passing sediment gravity flows travelled, with those channels feeding down-fan-located terminal mouth lobes (linear and sinuous architectures of BEV 10, Fig. 7A). The key observations for assessing by-pass are outlined in Stevenson *et al.* (2015), with *fpxbs* and *fmcs* being the key representative facies in this study (see Table 2), which are common in the 14/15-4Z intersection of Beverley (Fig. 17). It is possible that the by-passed proximal and medial areas during growth phase (II) act to preserve HEBs deposited during the growth phase (I), and therefore can potentially be used as by-pass indicators.

The abandonment phase (T5 of Fig. 20) reflects progressive reduction in sediment supply to the fan. Flows became smaller and less-energetic, resulting in a landward-retreat of facies belts, and deposition of more distal flow types above those of older proximal deposits (e.g. Hodgson *et al.*, 2006). Consequently, a well-developed coarse-grained abandonment phase is not necessarily deposited in the more distal areas.

The termination phase (T6 of Fig. 20) represents the final abandonment of the system, evidenced by a relatively abrupt change in sedimentation, and deposition of a thick (typically >1 m), laterally-extensive hemi-limnic mudstone drape. Interbedded, thin, very fine-grained sandstones encountered within this drape reflect either isolated sediment delivery from the fan feeders (i.e.

during a storm event), or the distal expression of laterally adjacent active systems. However, whilst the abrupt switch to mudstone deposition is classically associated with a rapid de-activation of fan systems (Pickering, 1983), recent studies suggest that it could be accounted for through "a combination of compensational stacking and rapid back-stepping of lobe elements" (Ferguson *et al.*, 2020). Because there is some component of compensational stacking in the Casper and Beverley fans, the latter model is entirely plausible.

Hybrid event bed spatial and temporal distribution within deep-lacustrine fan models

In terms of spatial distribution, HEBs are typically associated with lobe fringe and lobe distal fringe locations (Haughton *et al.*, 2003, 2009; Hodgson, 2009; Talling, 2013; Kane *et al.*, 2017; Spychala *et al.*, 2017a). When considering their temporal occurrences, examples from the Karoo Basin in South Africa show HEBs to be common in the initiation and growth phases, and relatively scarce during the fan retreat phase. Their prevalence in the initiation phase is thought to be related to "increased sediment supply and slope efficiency during the onset of sea-level fall" (Hodgson, 2009). They have also been documented within the Clare Shale and lowermost Ross Sandstone formations in Ireland, where they are attributed to widespread sea floor erosion and basin disequilibrium, steep slopes and a bias to recording or persevering HEBs in the distal Ross system (Haughton *et al.*, 2009; Pierce *et al.*, 2018). Other studies encountered HEBs throughout the initiation, growth and abandonment phases (Davis *et al.*, 2009; Fonnesu *et al.*, 2018). Their temporal position has been related to autocyclic and allocyclic controls, such as sea-level change, tectonism, sequence stratigraphical patterns and lobe switching (Haughton *et al.*, 2009; Hodgson, 2009; Spychala *et al.*, 2017b). Because all of these examples are from deep-marine basins, these concepts need to be validated, and to some extent established, for deep-lacustrine depositional models, where there are contrasting geological controls on flow processes and basin development (see discussion in Dodd *et al.*, 2019).

Hybrid event beds in the initiation phase
During the initiation phase (T1 of Fig. 20), the three fans preserve thin HEBs directly below lobe axis or lobe fringe deposits (see Figs 13A, 13B, 14F, 15 and 17). Moving upward through

the initiation phase of Zebedee (Fig. 15), HEBs become thicker and more complete in terms of H1–H5 divisions from the idealized sequence. This pattern reflects gradually increasing fan activity and associated sediment delivery, which eventually formed stacked lobe axis deposits during growth stages (Fig. 20), and suggests gradual progradation of the fan system (Hodgson *et al.*, 2006). The sedimentary logs characterize an area defined as a stranded lobe fringe area within Zebedee (Fig. 6B), showing that HEBs are typically encountered within the initiation phase in these locations (Figs 15 and 20). HEBs are observed directly below thick lobe axis deposits of Beverley, though note that the core-base terminates before the bottom of the sandy interval (Fig. 4). Beverley displays a stacked succession of HEBs, which show a thickening-upward trend, and in particular thickening of H1 with respect to H2 to H5, transitioning into the lobe axis deposits (Fig. 17). These HEBs were deposited in the distal fringes of early lobes, and were subsequently overlain and reworked by high-density turbidites of the terminal mouth lobe. HEBs and banded sandstones are preserved directly below lobe axis deposits in CA10 (Fig. 13A and F; *sensu* Stevenson *et al.*, 2020), which are both interpreted as being part of fringe deposits of early lobes that were later overstepped. Sandstone bed amalgamation in the overlying lobe axis deposits of the growth (I) phase suggests that this area later became dominated by high energy processes, with sinuous seismic amplitude architectures observed at the well location (Fig. 5).

Hybrid event beds formed during the initiation phase (T1 of Fig. 20) characterize deposition during the early stages of fan development (Haughton *et al.*, 2009; Hodgson, 2009; Pierce *et al.*, 2018). These HEBs reflect the highest potential for flow-scale palaeo-topographical interaction (*c.f.* scales observed in Hansen *et al.*, 2019), erosion (for example, see banded sandstones observed at the base of CA10 in Fig. 14F; *sensu* Stevenson *et al.*, 2020), inclusion of finer grained material from initial muddy substrates into flows (i.e. substrate de-lamination, *sensu* Fonnesu *et al.*, 2016), and associated flow deceleration (*sensu* Patacci *et al.*, 2014; Southern *et al.*, 2015; Baas *et al.*, 2021), which collectively act to drive mixed flow behaviour during the initiation phase.

When HEBs are absent in the initiation phase, they were either not deposited in those locations, or they were extensive during the initiation phase, but were later eroded and reworked during the growth phase (T2 and T3 of Fig. 20). The high possibility of erosion and re-working of HEBs in lobe axis areas results in significant potential for preservation bias towards fringe positions. Alternatively, flow focussing and the production of 'finger-like' geometries (*sensu* Prélat *et al.*, 2009; Groenenberg *et al.*, 2010; Hansen *et al.*, 2019) can result in hybrid beds being encountered in some areas of the fan during the initiation phase, whilst in other areas, HEB-absent Lobe Axis FA dominate, without models that invoke preservation bias to explain the observations.

Hybrid event beds in the growth phase

HEBs preserved in lobe axis deposits of the growth phase(s) (T2 and/or T3 of Fig. 20) appear to be less common and localized than during other times. Well 14/15b-5 (Fig. 15) intersects an area of low seismic amplitudes in the Zebedee Fan, previously interpreted as 'stranded lobe fringe areas' (Dodd *et al.*, 2019). It is interpreted that these areas represent enclosed remnants of early lobe fringe and lobe distal fringe deposition formed during the initiation phase that were left stranded as the fan built out (*sensu* Hodgson *et al.*, 2006). Alternatively, these areas represented small flow-scale palaeo-topographical highs, around which flows interacted. As flows were forced to decelerate against or around these highs, this likely would promote flow transformation and HEB development (e.g. McCaffrey & Kneller, 2001; Southern *et al.*, 2015; Bell *et al.*, 2018; Hansen *et al.*, 2019). On the basis of HEBs being observed throughout all fan phases elsewhere (e.g. Davis *et al.*, 2009; Kane *et al.*, 2017; Fonnesu *et al.*, 2018), it is quite likely that growth phase HEBs are more prevalent in more distal locations in the Casper, Beverley and Zebedee Fan systems, away from available well control.

Hybrid event beds in the abandonment phase

HEBs are prominent during the abandonment phase (T5 of Fig. 20). This is particularly the case at 14/10-9Z in CA10 (Fig. 13A), and at 14/15b-5 in Zebedee (Fig. 15). Well 14/10-9Z intersects CA10 in a sinuous lobe axis area (Fig. 5), and the HEBs encountered in this example (Fig. 13A) are interpreted as the distal

expression of up-dip flows, which progressively decreased in size, energy, velocity and volume during retreat (Fig. 20). HEB generation was promoted through flow deceleration, enhanced by the interaction with remaining flow-scale palaeo-topography, which was formed during the growth phases (for example, channels and lake-floor topography associated with compensational stacking of lobes). Well 14/15b-5 intersects Zebedee in a stranded lobe fringe area (Fig. 6), where more diverse flow types are expected due to variable flow-scale palaeotopography, and potentially elevated mud availability for erosion and entrainment.

By comparison, there is a complete lack of HEBs in the abandonment phase in 14/15-4Z through to CA20 (Fig. 13B), and deposition of Lobe Fringe FA terminates abruptly, switching to Hemi-Limnic Mudstones FA. Similarly, the Beverley interval in the same well (Fig. 17) has poorly-developed HEBs in the abandonment phase. Like with CA20, and despite its lobe axis position, the 14/15-4Z well intersects the Beverley Fan in a distal area (Fig. 7). The absence of HEBs in these two examples can be interpreted as the distal areas (see Figs 5 and 7) becoming sediment-starved as the fan shut down and facies belts retreated landward (Fig. 20). The abrupt switch from sandstones to mudstones during fan abandonment has been previously documented in Ferguson *et al.*, (2020), where this relationship was explained through "a combination of compensational stacking and rapid back-stepping of lobe elements". Certainly, the abrupt switch from sandstones to mudstones in CA20 and Beverley in the distal locations, and HEBs deposited and preserved in the abandonment phases of CA10 and Zebedee in comparatively more proximal locations, may go some way to confirming this as a model for the North Falklands Basin deep-lacustrine fan systems in this study.

CONCLUSIONS

Hybrid Event Beds (HEBs) are texturally and compositionally-diverse successions deposited by flows exhibiting 'mixed behaviour', which form complex successions of sandstone and mudstone, within deepwater settings. When comparing them with their marine counterparts, HEBs are an equally important component of deep-lacustrine fan systems. They comprise five internal units, including H1, H2, H3, H4 and H5. In particular,

the H3 unit can be divided into H3a, H3b and H3c sub-units, based on intra-H3 contacts, differences in mud-matrix content and textural variability. These sub-units are interpreted to have formed as a result of advanced rearward longitudinal transformation processes, leading to the along-flow segregation of the H3 debrite into multiple flow components. This is in contrast with the H3 unit more-typically related to rapid *en-masse* deposition throughout the debris flows length and width. HEBs are encountered and preserved in both Lobe Axis Facies Association (FA) and Lobe Fringe FA areas of the Casper, Zebedee and Beverley deep-lacustrine fans, and rarely within Hemi-Limnic Mudstones FA. Their presence can be better-explained when considered along with their temporal position during the development of each of these fans. In this dataset, HEBs are formed and preserved in: (i) the initiation phase, common and widely distributed; (ii) sometimes in the growth phase in certain areas across the fans surface (i.e. stranded lobe fringe areas and in fringe positions); and (iii) during the abandonment phase as facies belts retreated landward.

CONFLICT OF INTEREST

The authors declare no conflict of interest.

DATA AVAILABILITY STATEMENT

The data that support the findings of this study are available from Falkland Islands Government Department of Mineral Resources. Restrictions apply to the availability of these data, which were used under license for this study. Data are available https://www.fig.gov.fk/mineralresources/ with the permission of Falkland Islands Government.

REFERENCES

Allen, J.R.L. (1982) *Sedimentary Structures*. Elsevier, Amsterdam, 1–2 pp.

Allen, J.R.L. (1984) Parallel lamination developed from upper-stage plane beds: a model based on the larger coherent structures of the turbulent boundary layer. *Sed. Geol.*, **39**, 227–242.

Amy, L.A., Peachey, S.A., Gardiner, A.A. and Talling, P.J. (2009) Prediction of hydrocarbon recovery from turbidite sandstones with linked-debrite facies: Numerical flow-simulation studies. *Mar. Pet. Geol.*, **26**, 2032–2043.

Amy, L.A. and Talling, P.J. (2006) Anatomy of turbidites and linked debrites based on long distance (120 x 30 km) bed correlation, Marnoso Arenacea Formation, Northern Apennines, Italy. *Sedimentology*, **53**, 161–212.

Anderson, R.Y. and Dean, W.E. (1988) Lacustrine varve formation through time. *Palaeogeogr. Palaeoclimatol. Palaeoecol.*, **62**, 215–235.

Baas, J.H. (2004) Conditions for formation of massive turbiditic sandstones by primary depositional processes. *Sed. Geol.*, **166**, 293–310.

Baas, J.H., Best, J.L., Peakall, J. and Wang, M. (2009) A phase diagram for turbulent, transitional, and laminar clay suspension flows. *J. Sediment. Res.*, **79**, 162–183.

Baas, J.H., Best, J.L. and Peakall, J. (2011) Depositional processes, bedform development and hybrid bed formation in rapidly decelerated cohesive (mud-sand) sediment flows. *Sedimentology*, **58**, 1953–1987.

Baas, J.H., Tracey, N.D. and Peakall, J. (2021) Sole marks reveal deep-marine depositional process and environment: implications for flow transformation and hybrid-event-bed models. *J. Sediment. Res.*, **91**, 986–1009.

Baganz, O.W., Bartov, Y., Bohacs, K. and Nummedal, D. (Eds.) (2012) Lacustrine sandstone reservoirs and hydrocarbon systems. *AAPG Memoir*, **95**, 1–11.

Baker, M.L. and Baas, J.H. (2020) Mixed sand–mud bedforms produced by transient turbulent flows in the fringe of submarine fans: Indications of flow transformation. *Sedimentology*, **67**, 2645–2671.

Barker, S.P., Haughton, P.D.W., McCaffrey, W.D., Archer, S.G. and Hakes, B. (2008) Development of rheological heterogeneity in clay-rich high-density turbidity currents: Aptian Britannia Sandstone Member, U.K. Continental Shelf. *J. Sediment. Res.*, **78**, 45–68.

Bell, D., Stevenson, C.J., Kane, I.A., Hodgson, D.M. and Poyatos-Moré, M. (2018) Topographic controls on the development of contemporaneous but contrasting basin-floor depositional architectures. *J. Sediment. Res.*, **88**, 1166–1189.

Boulesteix, K., Poyatos-Moré, M., Flint, S.S., Taylor, K.G., Hodgson, D.M. and Hasiotis, S.T. (2019) Transport and deposition of mud in deep-water environments: Processes and stratigraphic implications. *Sedimentology*, **66**, 2894–2925.

Brooks, H., Hodgson, D.M., Brunt, R.L., Peakall, J.P., Hofstra, M. and Flint, S. (2018) Deep-water channel-lobe transition zone dynamics: Processes and depositional architecture, an example from the Karoo Basin, South Africa. *Geol. Soc. Am. Bull.*, **130**, 1723–1746.

Bunt, R. (2015) The use of seismic attributes for fan and reservoir definition in the Sea Lion Field, North Falkland Basin. *Petrol. Geosci.*, **21**, 137–149.

Burgess, P.M., Masiero, I., Toby, S.C. and Duller, R.A. (2019) A big fan of signals? Exploring autogenic and allogenic process and product in a numerical stratigraphic forward model of submarine-fan development. *J. Sediment. Res.*, **89**, 1–12.

Cartigny, M.J.B., Eggenhuisen, J.T., Hansen, E.W.M. and Postma, G. (2013) Concentration –dependent flow stratification in experimental high-density turbidity currents and their relevance to turbidite facies models. *J. Sediment. Res.*, **83**, 1047–1065.

Cronin, B.T., Dawson, K. and Jubilee Development Team (2018) Frontal splay geometry, distribution, connectivity and reservoir characterization in a mid-slope environment: The Jubilee Field, Offshore Ghana. AAPG Search and Discovery Article #51475, 09/04/2018.

Davis, C., Haughton, P., McCaffrey, W., Scott, E., Hogg, N. and Kitching, D. (2009) Character and distribution of hybrid sediment gravity flow deposits from the outer Forties Fan, Palaeocene Central North Sea, UKCS. *Mar. Pet. Geol.*, **26**, 1919–2939.

Davis, G., Newbould, R., Lopez, A., Hadibeik, H., Guevara, Z., Engelman, B., Balliet, R., Ramakrishna, S. and Imrie, A. (2018) An integrated formation evaluation approach to characterize a turbidite fan complex: case study, Falkland Islands. *SPWLA 59th Annual Logging Symposium Conference Paper, London.*

Dodd, T.J.H., McCarthy, D.J. and Richards, P.C. (2019) A depositional model for deep-lacustrine, partially confined, turbidite fans: Early Cretaceous, North Falkland Basin. *Sedimentology*, **66**(1), 53–80.

Dodd, T.J.H., McCarthy, D.J. and Clarke, S.M. (2020) Clastic injectites, internal structures and flow regime during injection: The Sea Lion Injectite System, North Falkland Basin. *Sedimentology*, **67**, 1014–1044.

Ferguson, R.A., Kane, I.A., Eggenhuisen, J.T., Pohl, F., Tilston, M., Spychala, Y.T. and Brunt, R.L. (2020) Entangled external and internal controls on submarine fan evolution: An experimental perspective. *Deposit. Rec.*, **6**, 605–624.

Fonnesu, M., Felletti, F., Haughton, P.D.W., Patacci, M. and McCafrey, W.D. (2018) Hybrid event bed character and distribution linked to turbidite sub-environments: The North Apennine Gottero Sandstone (north-west Italy). *Sedimentology*, **65**, 151–190.

Fonnesu, M., Haughton, P., Felletti, F. and McCaffrey, W. (2015) Short length-scale variability of hybrid event beds and its applied significance. *Mar. Pet. Geol.*, **67**, 583–603.

Fonnesu, M., Patacci, M., Haughton, P.D.W., Felletti, F. and McCaffrey, W.D. (2016) Hybrid event beds generated by local substrate delamination on a confined-basin floor. *J. Sediment. Res.*, **86**, 929–943.

Francis, A., Lewis, M. and Booth, C. (2015) Sea Lion Field, North Falkland Basin: seismic inversion and quantitative interpretation. *Petrol. Geosci.*, **21**, 151–169.

Groenenberg, R.M., Hodgson, D.M., Prélat, A., Luthi, S.M. and Flint, S. (2010) Flow-deposit interaction in submarine lobes: insights from outcrop observations and realizations of a process-based numerical model. *J. Sediment. Res.*, **80**, 252–267.

Hansen, L.A.S., Hodgson, D.M., Pontén, A., Bell, D. and Flint, S. (2019) Quantification of Basin-Floor Fan Pinchouts: Examples From the Karoo Basin, South Africa. *Front. Earth Sci.*, **7**, 12. https://doi.org/10.3389/feart.2019.00012.

Haughton, P.D.W., Barker, S.P. and McCaffrey, W.D. (2003) 'Linked' debrites in sand-rich turbidite systems – origin and significance. *Sedimentology*, **50**, 459–482.

Haughton, P., Davis, C., McCaffrey, W. and Barker, S. (2009) Hybrid sediment gravity flow deposits – Classification, origin and significance. *Mar. Pet. Geol.*, **26**, 1900–1918.

Hodgson, D.M. (2009) Distribution and origin of hybrid beds in sand-rich submarine fans of the *Tanqua depocentre*, Karoo Basin, South Africa. *Mar. Pet. Geol.*, **26**, 1940–1956.

Hodgson, D.M., Flint, S.S., Hodgetts, D., Drinkwater, N.J., Johannessen, E.P. and Luthi, S.M. (2006) Stratigraphic evolution of fine-grained submarine fan systems, Tanqua Depocenter, Karoo Basin, South Africa. *J. Sediment. Res.*, **76**, 20–40.

Holmes, N., Atkin, D., Mahdi, S. and Ayress, M. (2015) Intergarted biostratigraphy and chemical stratigraphy in the development of a reservoir-scale stratigraphic framework for the Sea Lion Field are, North Falkland Basin. *Petrol. Geosci.*, **21**, 171–182.

Horton, B.K. and Schmitt, J.G. (1996) Sedimentology of a lacustrine fan-delta system, Miocene Horse Camp Formation, Nevada, USA. *Sedimentology*, **43**, 133–155.

Hovikoski, J., Therkelsen, J., Nielsen, L.H., Bojesen-Koefoed, J.A., Nytoft, H.P., Petersen, H.I., Abatzis, I., Tuan, H.A., Phuong, B.T.N., Dao, C.V. and Fyhn, M.B.W. (2016) Density-flow deposition in a fresh-water lacustrine rift basin, Palaeogene Back Long Vi Grabem, Vietnam. *J. Sediment. Res.*, **86**, 982–1007.

Hussain, A., Haughton, P.D.W., Shannon, P.M., Turner, J.N., Pierce, C.S., Obradors-Latre, A., Barker, S.P. and Martinsen, O.J. (2020) High-resolution X-ray fluorescence profiling of hybrid events: Implications for sediment gravity flow behaviour and deposit structure. *Sedimentology*, **67**, 2850–2882.

Jones, D.J.R., McCarthy, D.J. and Dodd, T.J.H. (2019) Tectonostratigraphy and the petroleum systems in the Northern sector of the North Falkland Basin, South Atlantic. *Mar. Pet. Geol.*, **103**, 150–162.

Kane, I.A. and Pontén, A.S.M. (2012) Submarine transitional flow deposits in the Paleogene Gulf of Mexico. *Geology*, **40**, 1119–1122. https://doi.org/10.1130/G33410.1

Kane, I.A., Pontén, A.S.M., Vangal, B., Eggenhuisen, J.T., Hodgson, D.M. and Spychala, Y.T. (2017) The stratigraphic record and processes of turbidity current transformation across deep-marine lobes. *Sedimentology*, **64**, 1236–1273.

Lohr, T. and Underhill, J.R. (2015) Role of rift transection and punctuated subsidence in the development of the North Falkland Basin. *Petrol. Geosci.*, **21**, 85–110.

Lopez Marmolejo, A., Newbould, R., Lawton, L. and Godlewski, J. (2018) Integrated Dynamic Modelling of the Sea Lion Field. Paper presented at the SPE Europec featured at 80th EAGE Conference and Exhibition, Copenhagen, Denmark, pp. 1–16.

Lowe, D.R. (1979) Sediment gravity flows: their classification and some problems of application to natural flows and deposits. *SEPM Spec. Public.*, **27**, 75–82.

Lowe, D.R. (1982) Sediment gravity flows: II. Depositional models with special reference to the deposits of high-density turbidity currents. *J. Sediment. Petrol.*, **52**(1), 279–297.

Lowe, D.R. and Guy, M. (2000) Slurry-flow deposits in the Britannia Formation (Lower Cretaceous), North Sea: a new perspective on the turbidity current and debris flow problem. *Sedimentology*, **47**, 31–70.

MacAulay, F. (2015) Sea Lion Field discovery and appraisal: a turning point for the North Falkland Basin. *Petrol. Geosci.*, **21**, 111–124.

McCaffrey, W. and Kneller, B. (2001) Process controls on the development of stratigraphic trap potential on the margins of confined turbidite systems and aids to reservoir evaluation. *AAPG Bull.*, **85**(6), 971–988.

Mulder, T. and Alexander, J. (2001) The physical character of subaqueous sedimentary density flows and their deposits. *Sedimentology*, **48**, 269–299.

Mutti, E. and Nilsen, T.H. (1981) Significance of intraformational rip-up clasts in deep-sea fan deposits. *International Association of Sedimentologists 2nd European Meeting, Bologna (abstract)*.

Mutti, E. and Normark, W.R. (1987) Comparing examples of modern and ancient turbidite systems: problems and concepts. In: *Marine Clastic Sedimentology* (Eds Leggett, J.K. and Zuffa, G.G.), pp. 1–38. Graham and Trotman, London.

Pan, S., Liu, H., Xu, D., Wei, P., Qu, Y., Guan, X., Lu, C. and Zhang, S. (2020) Sublacustrine gravity-induced deposits: The diversity of external geometries and origins. *Sed. Geol.*, **407**, 105738.

Patacci, M., Haughton, P.D.W. and McCaffrey, W.D. (2014) Rheological complexity in sediment gravity flows forced to decelerate against a confining slope, Braux, SE France. *J. Sediment. Res.*, **84**, 270–277.

Patacci, M., Marini, M., Felletti, F., Di Giulio, A., Setti, M. and McCaffrey, W. (2020) Origin of mud in turbidites and hybrid event beds: insight from a ponded mudstone caps of the Castagnola turbidite system (north-west Italy). *Sedimentology*, **67**, 2625–2644.

Pickering, K.T. (1983) Transitional submarine fan deposits from the late Precambrian Kongsfjord Formation submarine fan, NE Finnmark, N. Norway. *Sedimentology*, **30**, 181–199.

Pierce, C.S., Haughton, P.D.W., Shannon, P.M., Pulham, A.J., Barker, S.P. and Martinsen, J. (2018) Variable character and diverse origin of hybrid event beds in a sandy submarine fan system, Pennsylvanian Ross Sandstone Formation, western Ireland. *Sedimentology*, **65**, 952–992.

Pierson, T.C. (1981) Dominant particle support mechanisms in debris flows at Mt Thomas, New Zealand, and implications for flow mobility. *Sedimentology*, **28**, 49–60.

Pierson, T.C. and Costa, J.C. (1987) A rheologic classification of subaerial sediment-water flows. *Geol. Soc. Am. Rev. Eng. Geol.*, **7**, 1–12.

Porten, K.W., Kane, I.A., Warchol, M.J. and Southern, S.J. (2016) A sedimentological process-based approach to depositional reservoir quality of deep-marine sandstones: an example from the Springar Formation, northwestern Voring Basin, Nowegian Sea. *J. Sediment. Res.*, **86**, 1269–1286.

Postma, G., Nemec, W. and Kleinspehn, K.L. (1988) Large floating clasts in turbidites: a mechanism for their emplacement. *Sed. Geol.*, **58**, 47–61.

Prélat, A., Hodgson, D.M. and Flint, S.S. (2009) Evolution, architecture and hierarchy of distributary deep-water deposits: a high-resolution outcrop investigation from the Permian Karoo Basin, South Africa. *Sedimentology*, **56**, 2132–2154.

Ricci Lucchi, F. and Valmori, E. (1980) Basin-wide turbidites in a Miocene, over-supplied deep-sea plain: a geometrical analysis. *Sedimentology*, **27**, 241–270.

Richards, P., Duncan, I., Phipps, C., Pickering, G., Grzywacz, J., Hoult, R. and Merritt, J. (2006) Exploring for

fan and delta sandstones in the offshore Falklands basins. *J. Pet. Geol.*, **29**, 199–214.

Richards, P.C. and **Fannin, N.G.T.** (1997) Geology of the North Falkland Basin. *J. Pet. Geol.*, **20**, 165–183.

Richards, P.C., **Gatliff, R.W.**, **Quinn, M.F.** and **Fannin, N.G.T.** (1996a) Petroleum Potential of the Falkland Islands Offshore Area. *J. Pet. Geol.*, **19**, 161–182.

Richards, P.C., **Gatliff, R.W.**, **Quinn, M.F.**, **Williamson, J.P.** and **Fannin, N.G.T.** (1996b) The geological evolution of the Falkland Islands continental shelf. In: *1996 Weddel Sea Tectonics and Gondwana Break-up* (Eds Storey, B.C., King, E.C. and Livermore, R.A.), *Geological Society Special Publication*, **108**, 105–128.

Richards, P.C. and **Hillier, B.V.** (2000) Post-drilling Analysis of the North Falkland Basin – Part 1: Tectono-Stratigraphic Framework. *J. Pet. Geol.*, **23**, 253–272.

Shan, X., **Yu, X.**, **Jin, L.**, **Li, Y.**, **Tan, C.**, **Li, S.** and **Wang, J.** (2020) (2020) Bed type and flow mechanism of deep water sub-lacustrine fan fringe facies: an example from the Middle Permian Lucaogou Formation in Southern Junggar Basin, NW China. *Petrol. Sci.*, **18**, 339–361.

Simm, R. and **Bacon, M.** (2014) *Seismic Amplitude: An Interpreter's Handbook*. Cambridge University Press.

Sohn, Y.K. (1997) On traction-carpet sedimentation. *J. Sediment. Res.*, **67**(3), 502–509.

Sohn, Y.K., **Choe, M.Y.** and **Jo, H.R.** (2002) Transition from debris flow to hyperconcentrated flow in a submarine channel (the Cretaceous Cerro Toro Formation, southern Chile). *Terra Nova*, **14**, 405–415.

Southern, S.J., **Kane, I.A.**, **Warchol, M.J.**, **Porten, W.** and **McCaffrey, W.D.** (2017) Hybrid event beds dominated by transitional-flow facies: character, distribution and significance in the Maastrichtian Springar Formation, north-west Vøring Basin, Norwegian Sea. *Sedimentology*, **64**, 747–776.

Southern, S.J., **Patacci, M.**, **Felletti, F.** and **McCaffrey, W.D.** (2015) Influence of flow containment and substrate entrainment upon sandy hybrid event beds containing a co-genetic mud-clast-rich division. *Sed. Geol.*, **321**, 105–122.

Spears, D.A. (2012) The origin of tonsteins, and overview, and links with seatearths, fireclays and fragmental clays rocks. *Int. J. Coal Geol.*, **94**, 22–31.

Spychala, Y.T., **Hodgson, D.M.**, **Prélat, A.**, **Kane, I.A.**, **Flint, S.S.** and **Mountney, N.P.** (2017a) Frontal and lateral submarine lobe fringes: comparing sedimentary facies, architecture and flow processes. *J. Sediment. Res.*, **87**, 75–96.

Spychala, Y.T., **Hodgson, D.M.** and **Lee, D.R.** (2017b) Autogenic controls on hybrid bed distribution in submarine lobe complexes. *Mar. Pet. Geol.*, **88**, 1078–1093.

Stevenson, C.J., **Jackson, C.A.L.**, **Hodgson, D.M.**, **Hubbard, S.M.** and **Eggenhuisen, J.T.** (2015) Deep-water sediment bypass. *J. Sediment. Res.*, **85**, 1058–1081.

Stevenson, C.J., **Peakall, J.**, **Hodgson, D.M.**, **Bell, D.** and **Privat, A.** (2020) Tb or not tb: banding in turbidite sandstone. *J. Sediment. Res.*, **90**, 821–842.

Stevenson, C.J., **Talling, P.J.**, **Sumner, E.J.**, **Masson, D.G.**, **Frenz, M.** and **Wynn, R.B.** (2014) On how thin submarine flows transported large volumes of sand for hundreds of kilometres across a flat basin plain without eroding the sea floor. *Sedimentology*, **61**, 1982–2019.

Stow, D.A.V. and **Tabrez, A.R.** (1998) Hemipelagites: processes, facies and model. In: *Geological Processes on Continental Margins: Sedimentation, Mass-Wasting and Stability* (Eds Stoker, M.S., Evans, D. and Cramp, A.), *Geological Society, London, Special Publications*, **129**, 317–337.

Sumner, E.J., **Amy, L.A.** and **Talling, P.J.** (2008) Deposit structure and processes of sand deposition from decelerating sediment suspensions. *J. Sediment. Res.*, **78**, 529–547.

Sumner, E.J., **Talling, P.J.** and **Amy, L.A.** (2009) Deposits of flows transitional between turbidity current and debris flow. *Geology*, **37**, 991–994.

Sumner, E.J., **Talling, P.J.**, **Amy, L.A.**, **Wynn, R.B.**, **Stevenson, C.J.** and **Frenz, M.** (2012) Facies architecture of individual basin-plain turbidites: Comparison with existing models and implications for flow processes. *Sedimentology*, **59**, 1850–1887.

Talling, P.J. (2013) Hybrid submarine flows comprising turbidity current and cohesive debris flow: Deposits, theoretical and experimental analyses, and generalized models. *Geosphere*, **9**, 460–488.

Tan, M., **Zhu, X.**, **Geng, M.**, **Zhu, S.** and **Liu, W.** (2017) The occurrence and transformation of lacustrine sediment gravity flow related to depositional variation and palaeoclimate in the Lower Cretaceous Prosopis Formation of the Bongor Basin, Chad. *J. Afr. Earth Sc.*, **34**, 134–148.

Terlaky, V. and **Arnott, R.W.C.** (2014) Matrix-rich and associated matrix-poor sandstones: Avulsion splays in slope and basin-floor strata. *Sedimentology*, **61**, 1175–1197.

Tinterri, R. and **Piazza, A.** (2019) Turbidites facies response to the morphological confinement of a foredeep (Cervarola Sandstones Formation, Miocene, northern Apennines, Italy). *Sedimentology*, **66**, 636–674.

Walker, R.G. (1965) The origin and significance of the internal sedimentary structures of turbidites. *Proc. Yorkshire Geol. Soc.*, **35**, 1–32.

Williams, L.S. (2015) Sedimentology of the Lower Cretaceous reservoirs of the Sea Lion Field, North Falkland Basin. *Petrol. Geosci.*, **21**, 183–198.

Wynn, R.B., **Kenyon, N.H.**, **Masson, D.G.**, **Stow, D.A.V.** and **Weaver, P.P.E.** (2002) Characterization and recognition of deep-water channel-lobe transition zones. *AAPG Bulletin*, **86**, 1441–1462.

Yang, T., **Cao, Y.**, **Liu, K.**, **Wang, Y.**, **Zavala, C.**, **Friis, H.**, **Song, M.**, **Yuan, G.**, **Liang, C.**, **Xi, K.** and **Wang, J.** (2019) Genesis and depositional model of subaqueous sediment gravity-flow deposits in a lacustrine rift basin as exemplified by the Eocene Shahejie Formation in Jiyang Depression, Eastern China. *Mar. Pet. Geol.*, **102**, 231–257.

Zhang, L.F. and **Dong, D.Z.** (2020) Thickening-upward cycles in deep-marine and deep-lacustrine turbidite lobes: examples from the Clare Basin and the Ordos Basin. *J. Palaeogeogr.*, **9**, 1–16. https://doi.org/10.1186/s42501-020-00059-9

Zhang, X., **Zhu, X.**, **Lu, Z.**, **Lin, C.**, **Wang, X.**, **Pan, R.**, **Geng, M.** and **Xue, Y.** (2019) An early Eocene subaqueous fan system in the steep slope of lacustrine rift basins, Dongying Depression, Bohai Bay Basin, China.: Depositional character, evolution and geomorphology. *J. Asian Earth Sci.*, **171**, 28–45.